

Quantum Thermal Machines Improved by Internal Coupling: From Equilibrium to Non-equilibrium Limit Cycles

Jingyi Gao

Department of Physics, the University of Tokyo

5-1-5 Kashiwanoha, Kashiwa, Chiba, 277-8574, Japan.

Naomichi Hatano

Institute of Industrial Science, the University of Tokyo

5-1-5 Kashiwanoha, Kashiwa, Chiba, 277-8574, Japan

(Dated: March 3, 2026)

We investigate how internal coupling influences the operation and performance of a quantum Otto cycle operating as the Gibbs-state limit cycle (GSLC), equilibrating limit cycle (ELC), and non-equilibrating limit cycle (NELC). We show that the internal coupling significantly broadens the operational regime of the cycle. In particular, in parameter regimes where the uncoupled Otto cycle fails to operate as any thermal machine, the coupled system can function as an engine or a refrigerator. For the GSLC, in which we assume that the system quickly equilibrates during the isochoric processes, the internal coupling not only shifts and enlarges the operational regime but also enhances the efficiency and the coefficient of performance (COP), allowing the performance to exceed the standard Otto bounds while remaining below the Carnot limit. For ELC and NLEC, we validate the global approach of the Gorini–Kossakowski–Sudarshan–Lindblad (GKSL) master equation by comparison with the GSLC, and examine the NELC for finite interaction time and the ELC for

infinite interaction time. Although the efficiency and COP of NELC are lower than those of ELC, shorter interaction times yield higher power output, consistent with the power-efficiency trade-off.

I. Introduction

Quantum thermal machines have emerged as a central topic in quantum thermodynamics [1–4]. Compared to the classical thermal machine, the advantages of quantum thermal machines are often attributed to the quantum effect, which can potentially improve performance [5–8].

Among various types of quantum thermal models, the quantum Otto cycle [9–11] offers a particularly transparent framework for examining work extraction, heat flows, and thermodynamic performance in driven quantum systems. In standard formulations [12–14], the working medium is typically assumed to exhibit well-separated energy levels without internal couplings, allowing the cycle to be described solely in terms of dynamics due to externally controlled strokes. Under these assumptions, the fundamental performance bounds, such as the Otto efficiency and the coefficient of performance (COP), follow directly from the level separations and bath temperatures [15–18]. However, realistic quantum systems often involve non-negligible internal coupling between energy levels, arising from coherent interactions, external fields, or intrinsic device architecture. Such internal couplings can be a significant factor causing the quantum effect [19–21].

Several works have been published on the improved performance of coupled thermal machines [22–25]. However, all of them focused on the coupling between several subsystems, which is influenced not only by internal coupling but also by the system’s scale. Detailed analyses of the role of internal coupling in determining the operational regime, performance

bounds, and steady-state behaviors remain insufficiently explored. In particular, systematic analyses comparing thermalized equilibrium systems with non-equilibrium systems [26–28] obtained from microscopic treatments of open systems lack a thorough discussion.

In this work, we first systematically investigate how the internal coupling affects the operation, which is universal for all single-qubit quantum Otto cycles with internal coupling. On one hand, we analytically examine the influence of internal coupling on the operation regimes and performance of thermal machines. On the other hand, we present two representative cases in which the coupled quantum Otto cycle can operate as a thermal machine, but the uncoupled one cannot because no work would be exchanged with the environment without the internal couplings.

We consider three cases, namely the Gibbs-state limit cycle (GSLC), the equilibrating limit cycle (ELC), and the non-equilibrating limit cycle (NELC), to analyze the internally coupled quantum Otto thermal machines from equilibrium to non-equilibrium dynamics. In the Gibbs-state limit cycle (GSLC), we assume that the system rapidly reaches a thermal-equilibrium with each heat bath in every isochoric stroke of the limit cycle, ignoring the influence of the interaction time. The system states are always Gibbs states in the limit cycle, as shown in Fig. 1(a). Based on analytical and numerical calculations of the GSLC, we confirm that the internal coupling can not only broaden the operational regime of the quantum Otto cycle but also allow the thermal machines to exceed the standard Otto bounds while still respecting the Carnot limit.

However, an open quantum system can take a long time to equilibrate, and non-equilibrium processes are inevitable in practice. Regarding the internal system and the external heat baths as an open quantum system, we define the equilibrating limit cycle (ELC) with long interaction time in the isochoric processes, as shown in Fig. 1(b), and the

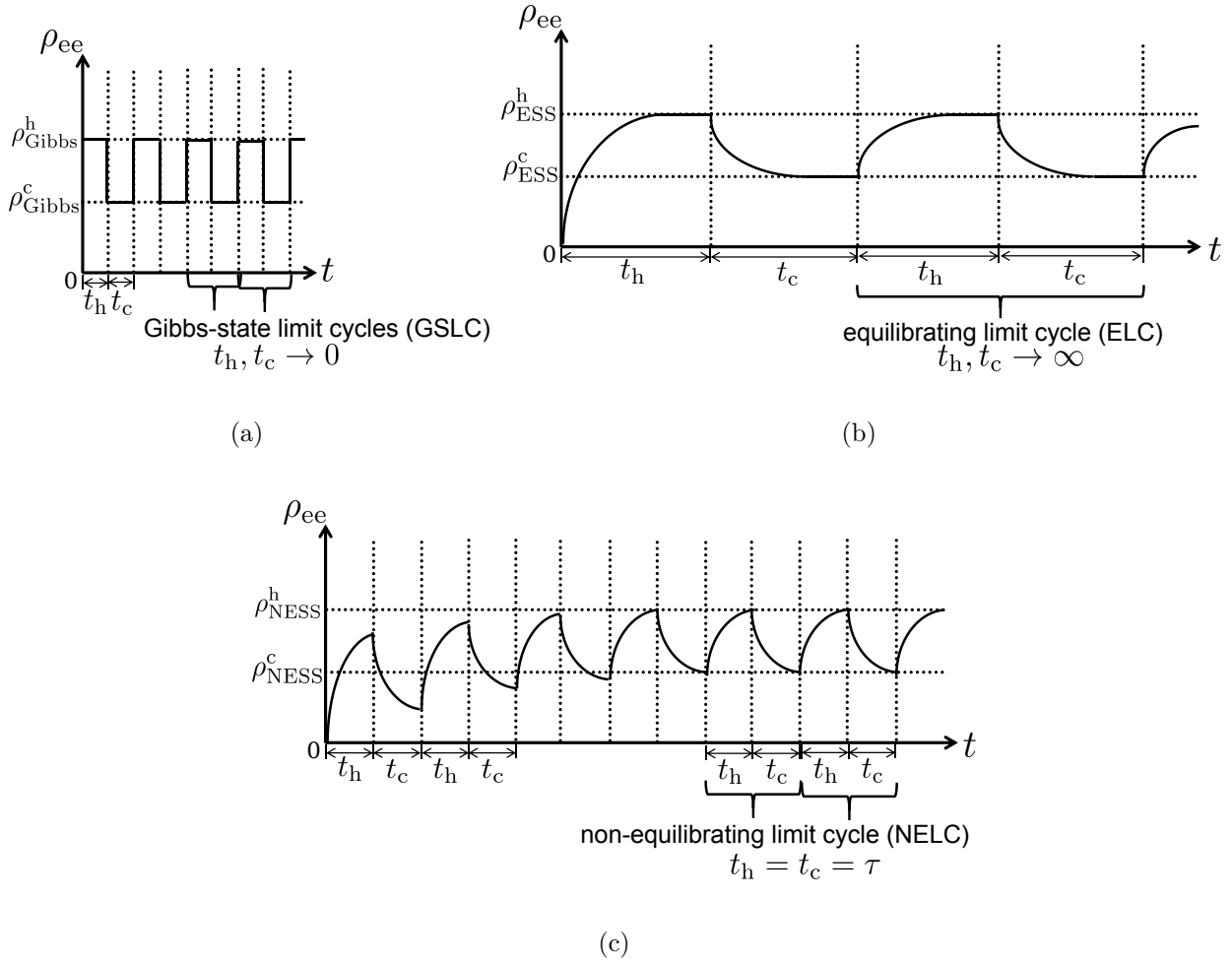


FIG. 1. Diagram of the system evolution of the (a) Gibbs-state limit cycle (GSLC), (b) equilibrating limit cycle (ELC), and (c) non-equilibrating limit cycle (NELC). For the GSLC in the panel (a), we do not consider the influence of the interaction time and assume that the system equilibrates rapidly in each isochoric process. Considering the Otto cycle as an open quantum system, it takes time for the system to equilibrate in each isochoric process. When the interaction time is short, the system state cannot reach the steady state in each isochoric process, but converges to the NELC as in panel (c). After the interaction time approaches infinity, the system equilibrates in each isochoric process and operates as the ELC in the panel (b).

non-equilibrating limit cycle (NELC) with short interaction time, as shown in Fig. 1(c). When the system does not equilibrate quickly, but if the interaction time is sufficiently long and the approaches equilibrium in each isochoric process, the operation converges to the ELC, regardless of the initial state. However, with a short interaction time, the system cannot equilibrate in each isochoric process. After several cycles, the operation converges to the NELC rather than the ELC, as schematically shown in Fig. 1(c).

By comparing the ELC with the GSLC, we confirm the validity of the global approach of the Gorini–Kossakowski–Sudarshan–Lindblad (GKSL) master equation [29–31]. From NELC to ELC, we observe that finite interaction times introduce a power-efficiency trade-off [32, 33]. Short interaction times yield reduced efficiency and COP, but higher power output, while long interaction times recover the equilibrium behavior with vanishing power. These findings collectively establish the internal coupling as a powerful and previously underappreciated resource for extending operational regimes, enhancing performance, and shaping non-equilibrium thermodynamic behavior in quantum thermal machines.

The present paper is organized as follows. In Sec. II, we review the quantum Otto cycle without internal coupling. In Sec. III, first, we introduce the internal coupling between the ground and excited energy levels of the qubit and analyze the influence of the coupling strengths on the efficiency of the engine and the coefficient of performance (COP) of the refrigerator, by comparing them to the performance of the quantum Otto cycle without internal coupling. Second, in the operation regime of thermal machines, we demonstrate two special cases in which the quantum Otto cycle with the internal coupling can operate as a thermal machine, but the one without it cannot, since no work would be exchanged between the internal system and the external environment without the coupling. After introducing the internal coupling, the system can operate as diverse types of thermal machines, depend-

ing on the coupling strength. In short, the internal coupling can extend the operation regime of the quantum Otto cycle. In Sec. IV, using the GSLC in Fig. 1(a), we calculate the influence of the internal coupling strength on the physical quantities, and numerically confirm that the internal coupling updates the operation regime and improves the performance. In Sec. V, considering the interaction time in the isochoric processes, we examine the NELC in Fig. 1(c) given by a short interaction time, and the ELC in Fig. 1(b) with a long interaction time. With a short interaction time, the efficiency and COP are low, whereas the power is high. Conversely, for a long interaction time, the efficiency and COP are high, whereas the power is low. After an infinite interaction time, the NELC converges to ELC, which exhibits the same phenomena as the Gibbs state. Finally, we conclude our analyses and results in Sec. VI. Besides, in Appendix B, we derive the eigensystems using the local and global GKSL master equations [29–31] and confirm the validity of the global approach. In Appendix A, the convergence to the NELC with short interaction time is confirmed by the quantum Perron–Frobenius theorem, since the transformation in each isochoric process is a primitive, completely positive and trace preserving (CPTP) map.

II. Review: Quantum Otto Cycle Without Coupling

The quantum Otto cycle consists of four strokes: a pair of isochoric processes and a pair of adiabatic processes, as illustrated in Fig. 2. During each isochoric stroke, labeled (a) and (c) in the figure, we keep the Hamiltonian of the internal two-level system constant, and the system state evolves due to interaction with the external baths with the inverse temperatures β_h and β_c , leading to heat flows. Conversely, during each adiabatic stroke, labeled (b) and (d) in the figure, the system state remains unchanged, while we vary the system Hamiltonian, leading to work production or extraction.

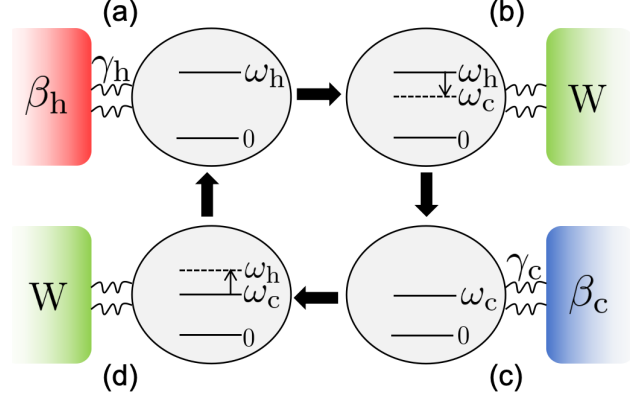


FIG. 2. Schematic view of quantum Otto cycle without any internal couplings. The internal system is a two-level system with excited energy level alternates between ω_h and ω_c . In the isochoric processes (a) and (c), it interacts with heat baths with the inverse temperature β_h and β_c , respectively. In the adiabatic processes (b) and (d), it interacts with the work storage denoted by W . We assume that the interaction time in the adiabatic processes is negligible.

For each of the isochoric processes (a) and (c) in Fig. 2, the total Hamiltonian is composed of three parts: the Hamiltonian of the internal two-level system, the Hamiltonian of the heat baths with the inverse temperature β_α , and the interaction Hamiltonian:

$$H = H_S^\alpha + H_B^\alpha + H_I^\alpha, \quad (1)$$

where $\alpha = h, c$ denotes the isochoric processes (a) and (c) in Fig. 2, respectively. The system Hamiltonian is given by

$$H_S^\alpha = \omega_\alpha \sigma_S^+ \sigma_S^- = \begin{pmatrix} 0 & 0 \\ 0 & \omega_\alpha \end{pmatrix}, \quad (2)$$

The heat baths are assumed to be bosonic, and thus the Hamiltonian H_B^α of each bath $\alpha = h, c$ is

$$H_B^\alpha = \sum_k \hat{b}_\alpha^\dagger \hat{b}_\alpha. \quad (3)$$

The interaction Hamiltonian between the system and the bath α takes the standard form:

$$H_I^\alpha = \sum_{k,\alpha} V_{k,\alpha} \sigma_S^x (\hat{b}_\alpha + \hat{b}_\alpha^\dagger). \quad (4)$$

For the state of the system, let us introduce the notation

$$\rho^\alpha = \begin{bmatrix} \rho_{gg}^\alpha & \rho_{ge}^\alpha \\ \rho_{eg}^\alpha & \rho_{ee}^\alpha \end{bmatrix} \text{ for } \alpha = \text{h, c.}$$

The system state is ρ^{h} after the isochoric process (a), while ρ^{c} after the process (c). The heat absorbed by the system from each bath $\alpha = \text{h, c}$ during the corresponding isochoric process is given by

$$Q_{\text{h}} = \text{Tr}[H_S^{\text{h}}(\rho^{\text{h}} - \rho^{\text{c}})] = \omega_{\text{h}}(\rho_{ee}^{\text{h}} - \rho_{ee}^{\text{c}}), \quad (5)$$

$$Q_{\text{c}} = \text{Tr}[H_S^{\text{c}}(\rho^{\text{c}} - \rho^{\text{h}})] = \omega_{\text{c}}(\rho_{ee}^{\text{c}} - \rho_{ee}^{\text{h}}). \quad (6)$$

Note that we define it such that the heat flows from the bath to the system when it is positive.

For the adiabatic processes (b) and (d) in Fig. 2, the work extracted from the environment into the internal system is given by

$$W_1 = \text{Tr}[(H_S^{\text{c}} - H_S^{\text{h}})\rho^{\text{h}}] = (\omega_{\text{c}} - \omega_{\text{h}})\rho_{ee}^{\text{h}}, \quad (7)$$

$$W_2 = \text{Tr}[(H_S^{\text{h}} - H_S^{\text{c}})\rho^{\text{c}}] = (\omega_{\text{h}} - \omega_{\text{c}})\rho_{ee}^{\text{c}}. \quad (8)$$

Note that we also define such that the work comes into the system when it is positive.

Therefore, the first law of thermodynamics holds in the form

$$W = W_1 + W_2 = -(\omega_{\text{h}} - \omega_{\text{c}})(\rho_{ee}^{\text{h}} - \rho_{ee}^{\text{c}}) = -(Q_{\text{h}} + Q_{\text{c}}). \quad (9)$$

For the standard Otto cycle, the inverse temperatures β_α and the energy levels ω_α are assumed to be positive. We also assume that $\beta_{\text{h}} < \beta_{\text{c}}$. The standard Otto cycle operates as

a heat engine when $\omega_h/\omega_c < \beta_c/\beta_h$, with the equilibrium efficiency given by

$$\eta_{\text{Otto}} = 1 - \frac{\omega_c}{\omega_h}. \quad (10)$$

Conversely, the cycle functions as a refrigerator when $\omega_h/\omega_c > \beta_c/\beta_h$, with the equilibrium coefficient of performance (COP)

$$\xi_{\text{Otto}} = \frac{\omega_c}{\omega_h - \omega_c}. \quad (11)$$

When $\omega_h/\omega_c = \beta_c/\beta_h$ or $\omega_c = \omega_h$, the system cannot operate as a thermal machine, since the energy absorbed from the hot bath equals the energy released to the cold bath and no work is produced.

III. Quantum Otto Cycle With Internal Coupling

A. Model and Dynamics

After introducing internal couplings into the system, as shown in Fig. 3, we can control not only the excited energy level of the internal system but also the internal coupling strength between the ground and the excited energy levels during the adiabatic processes. Hence, the internal coupling plays a significant role in determining the performance of the Otto cycle.

Introducing the internal coupling, we update the Hamiltonian of the internal system from Eq. (2) to

$$H_S^\alpha = \begin{pmatrix} 0 & g_\alpha \\ g_\alpha & \omega_\alpha \end{pmatrix}, \quad (12)$$

where $\alpha = h, c$ corresponds to the hot and cold isochoric strokes, respectively. Meanwhile, we keep the bath and interaction Hamiltonians in Eqs. (3) and (4) as they are, assuming

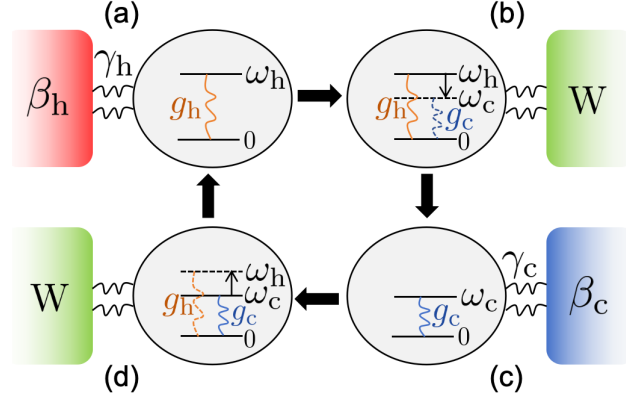


FIG. 3. Schematic view of quantum Otto cycle with the internal coupling between the excited and ground energy levels of the internal two-level system. The internal coupling strength is g_h and g_c in the isochoric process (a) and (c), respectively. In the adiabatic processes (b) and (d), not only do the excited energy levels alternate between ω_h and ω_c , but also the internal coupling strengths alternate between g_h and g_c .

that the external environment and the system-bath interaction are unaffected by the internal coupling g_α .

Consequently, after introducing the internal coupling, the total heat absorbed from each bath $\alpha = h, c$ during each isochoric process contains a contribution associated with the internal coupling strength, as in

$$Q_h = \text{Tr} [H_S^h(\rho^h - \rho^c)] \quad (13)$$

$$= g_h [(\rho_{eg}^h - \rho_{eg}^c) + (\rho_{ge}^h - \rho_{ge}^c)] + \omega_h(\rho_{ee}^h - \rho_{ee}^c), \quad (14)$$

$$Q_c = \text{Tr} [H_S^c(\rho^c - \rho^h)] \quad (15)$$

$$= g_c [(\rho_{eg}^c - \rho_{eg}^h) + (\rho_{ge}^c - \rho_{ge}^h)] + \omega_c(\rho_{ee}^c - \rho_{ee}^h). \quad (16)$$

In each adiabatic process, the total work extracted from the environment is given by

$$W_1 = \text{Tr}[(H_S^c - H_S^h)\rho^h] \quad (17)$$

$$= (\rho_{eg}^h + \rho_{ge}^h)(g_c - g_h) + (\omega_c - \omega_h)\rho_{ee}^h, \quad (18)$$

$$W_2 = \text{Tr}[(H_S^h - H_S^c)\rho^c] \quad (19)$$

$$= (\rho_{eg}^c + \rho_{ge}^c)(g_h - g_c) + (\omega_h - \omega_c)\rho_{ee}^c, \quad (20)$$

and the total work is given by

$$W = W_1 + W_2 = -(g_h - g_c) [(\rho_{eg}^h - \rho_{eg}^c) + (\rho_{ge}^h - \rho_{ge}^c)] - (\omega_h - \omega_c)(\rho_{ee}^h - \rho_{ee}^c) = -(Q_h + Q_c), \quad (21)$$

which respects the first law of thermodynamics. Note again that positive energy flows are defined as the heat absorption and the work extraction from the environment to the internal system.

We define that the Otto cycle operates as an engine when the energy flows as $Q_h > 0$, $Q_c < 0$, and $W < 0$. Its efficiency $\eta_{cp} = -W/Q_h$ is given by

$$\eta_{cp} = \frac{(g_h - g_c) [(\rho_{eg}^h - \rho_{eg}^c) + (\rho_{ge}^h - \rho_{ge}^c)] + (\omega_h - \omega_c)(\rho_{ee}^h - \rho_{ee}^c)}{g_h [(\rho_{eg}^h - \rho_{eg}^c) + (\rho_{ge}^h - \rho_{ge}^c)] + \omega_h(\rho_{ee}^h - \rho_{ee}^c)} \quad (22)$$

$$= 1 - F_A \frac{\omega_c}{\omega_h}, \quad (23)$$

where

$$F_A = \frac{\frac{g_c}{\omega_c}(f(g_h, \beta_h, \omega_h) - f(g_c, \beta_c, \omega_c)) + (\rho_{ee}^h - \rho_{ee}^c)}{\frac{g_h}{\omega_h}(f(g_h, \beta_h, \omega_h) - f(g_c, \beta_c, \omega_c)) + (\rho_{ee}^h - \rho_{ee}^c)}, \quad (24)$$

and the function

$$f(g_\alpha, \beta_\alpha, \omega_\alpha) = \rho_{ge}^\alpha + \rho_{eg}^\alpha \quad (25)$$

denotes the sum of the off-diagonal elements, which depends on the internal coupling strength g_α , the inverse temperature β_α , and the energy spacing ω_α in the isochoric process $\alpha = h, c$.

Let us stress here that the internal coupling g_α generates off-diagonal coherence to the system state.

Compared to the standard Otto efficiency $\eta_{\text{Otto}} = 1 - \omega_c/\omega_h$ without the internal coupling, after introducing the internal coupling, the efficiency η_{cp} can be either greater or less than η_{Otto} , because $F_A < 1$ or $F_A > 1$, depending on the six parameters $\{\omega_h, \omega_c, g_h, g_c, \beta_h, \beta_c\}$, as summarized in Table I. When $f(g_h, \beta_h, \omega_h) > f(g_c, \beta_c, \omega_c)$ and $g_h/\omega_h > g_c/\omega_c$, or when $f(g_h, \beta_h, \omega_h) < f(g_c, \beta_c, \omega_c)$ and $g_h/\omega_h < g_c/\omega_c$, the efficiency of the internally coupled system can surpass that of the standard Otto engine without the internal coupling. For a system with fixed bath temperatures β_α and energy levels ω_α , we can always adjust the internal coupling strengths g_α to achieve a higher efficiency, as shown in Table I.

	$f(g_h, \beta_h, \omega_h) < f(g_c, \beta_c, \omega_c)$	$f(g_h, \beta_h, \omega_h) = f(g_c, \beta_c, \omega_c)$	$f(g_h, \beta_h, \omega_h) > f(g_c, \beta_c, \omega_c)$
$g_h/\omega_h < g_c/\omega_c$	$\eta_{\text{cp}} > \eta_{\text{Otto}}$	$\eta_{\text{cp}} = \eta_{\text{Otto}}$	$\eta_{\text{cp}} > \eta_{\text{Otto}}$
$g_h/\omega_h = g_c/\omega_c$	$\eta_{\text{cp}} = \eta_{\text{Otto}}$	$\eta_{\text{cp}} = \eta_{\text{Otto}}$	$\eta_{\text{cp}} = \eta_{\text{Otto}}$
$g_h/\omega_h > g_c/\omega_c$	$\eta_{\text{cp}} < \eta_{\text{Otto}}$	$\eta_{\text{cp}} = \eta_{\text{Otto}}$	$\eta_{\text{cp}} < \eta_{\text{Otto}}$

TABLE I. Efficiency of the Otto engine with coupling η_{cp} , compared to the Otto efficiency η_{Otto} , given by $f(g_\alpha, \beta_\alpha, \omega_\alpha)$ and the relations between g_h/ω_h and g_c/ω_c .

Similarly, we define that the quantum Otto cycle runs as a refrigerator, when the energy flows as $Q_h < 0$, $Q_c > 0$, and $W > 0$. Its coefficient of performance (COP) $\xi_{\text{cp}} = Q_c/W$ is given by

$$\xi_{\text{cp}} = \frac{g_c [(\rho_{\text{eg}}^c - \rho_{\text{eg}}^h) + (\rho_{\text{ge}}^c - \rho_{\text{ge}}^h)] + \omega_c(\rho_{\text{ee}}^c - \rho_{\text{ee}}^h)}{(g_c - g_h) [(\rho_{\text{eg}}^h - \rho_{\text{eg}}^c) + (\rho_{\text{ge}}^h - \rho_{\text{ge}}^c)] + (\omega_c - \omega_h)(\rho_{\text{ee}}^h - \rho_{\text{ee}}^c)} \quad (26)$$

$$= \frac{\omega_c}{\omega_h - \omega_c} F_B, \quad (27)$$

where

$$F_B = \frac{\frac{g_c}{\omega_c}(f(g_c, \beta_c, \omega_c) - f(g_h, \beta_h, \omega_h)) + (\rho_{ee}^c - \rho_{ee}^h)}{\frac{g_h - g_c}{\omega_h - \omega_c}(f(g_c, \beta_c, \omega_c) - f(g_h, \beta_h, \omega_h)) + (\rho_{ee}^c - \rho_{ee}^h)}. \quad (28)$$

The comparison between the COP ξ_{cp} of the internally coupled system and the standard Otto COP $\xi_{Otto} = \omega_c/(\omega_h - \omega_c)$ is summarized in Table II.

	$f(g_h, \beta_h, \omega_h) < f(g_c, \beta_c, \omega_c)$	$f(g_h, \beta_h, \omega_h) = f(g_c, \beta_c, \omega_c)$	$f(g_h, \beta_h, \omega_h) > f(g_c, \beta_c, \omega_c)$
$(g_h - g_c)/(\omega_h - \omega_c) < g_c/\omega_c$	$\xi_{cp} > \xi_{Otto}$	$\xi_{cp} = \xi_{Otto}$	$\xi_{cp} < \xi_{Otto}$
$(g_h - g_c)/(\omega_h - \omega_c) = g_c/\omega_c$	$\xi_{cp} = \xi_{Otto}$	$\xi_{cp} = \xi_{Otto}$	$\xi_{cp} = \xi_{Otto}$
$(g_h - g_c)/(\omega_h - \omega_c) > g_c/\omega_c$	$\xi_{cp} < \xi_{Otto}$	$\xi_{cp} = \xi_{Otto}$	$\xi_{cp} > \xi_{Otto}$

TABLE II. The COP of the system with coupling ξ_{cp} , compared to the Otto COP ξ_{Otto} , given by $\text{sgn}([f(g_h, \beta_h, \omega_h) - f(g_c, \beta_c, \omega_c)])$ and the relations of $g_c/\omega_c > (g_h - g_c)$ and $(\omega_h - \omega_c)$.

The standard Otto COP ξ_{Otto} represents the equilibrium COP in the absence of the internal coupling. When $f(g_h, \beta_h, \omega_h) > f(g_c, \beta_c, \omega_c)$ and $(g_h - g_c)/(\omega_h - \omega_c) > g_c/\omega_c$ or $f(g_h, \beta_h, \omega_h) < f(g_c, \beta_c, \omega_c)$ and $(g_h - g_c)/(\omega_h - \omega_c) < g_c/\omega_c$, the COP of the internally coupled system can surpass the standard Otto value. Similarly to the engine case, for fixed bath temperatures β_α and energy spacings ω_α , the internal coupling strengths g_α can be tuned to achieve enhanced performance, as shown in Table II.

B. Special Cases

To emphasize the significance of the internal couplings, based on the analysis of the dynamics with internal coupling in Sec. III A, we discuss two special cases in which the Otto cycle would not function as a thermal machine without the internal coupling.

The first case occurs when the energy levels remain fixed, that is, $\omega_h = \omega_c = \omega$. Without

the coupling, the Otto cycle obviously would not produce any work. Even in this case, when the coupling strengths differ as $g_h \neq g_c$, the Otto cycle can operate as a thermal machine.

The heat currents and work in Eqs. (13)-(21) are reduced to

$$Q_h = g_h [(\rho_{eg}^h - \rho_{eg}^c) + (\rho_{ge}^h - \rho_{ge}^c)] + \omega(\rho_{ee}^h - \rho_{ee}^c) \quad (29)$$

$$= g_h (f(g_h, \beta_h, \omega) - f(g_c, \beta_c, \omega)) + \omega(\rho_{ee}^h - \rho_{ee}^c), \quad (30)$$

$$Q_c = g_c [(\rho_{eg}^c - \rho_{eg}^h) + (\rho_{ge}^c - \rho_{ge}^h)] + \omega(\rho_{ee}^c - \rho_{ee}^h) \quad (31)$$

$$= -g_c (f(g_h, \beta_h, \omega) - f(g_c, \beta_c, \omega)) - \omega(\rho_{ee}^h - \rho_{ee}^c), \quad (32)$$

$$W = -(g_h - g_c)(f(g_h, \beta_h, \omega) - f(g_c, \beta_c, \omega)). \quad (33)$$

In this case, the energy exchanges within the cycle are determined by five parameters: the inverse temperatures β_α of the baths, the coupling strengths g_α during each isochoric process, and the fixed energy level ω . The efficiency of the engine and the coefficient of performance (COP) of the refrigerator, given in Eqs. (22)–(26), now take the forms

$$\eta_{cp} = 1 - \frac{g_c}{g_h}, \quad (34)$$

$$\xi_{cp} = \frac{g_c}{g_h - g_c}. \quad (35)$$

Thus, when the energy levels are fixed, the operation and performance of the Otto cycle are governed solely by the internal coupling strengths g_α . Analogous to the standard Otto cycle without internal coupling, for which the engine operates when $1 > \omega_c/\omega_h > \beta_h/\beta_c$ and functions as a refrigerator when $1 > \beta_h/\beta_c > \omega_c/\omega_h$, the coupled system operates as an engine when $1 > g_c/g_h > \beta_h/\beta_c$ and as a refrigerator when $1 > \beta_h/\beta_c > g_c/g_h$ for the fixed energy level $\omega_h = \omega_c = \omega$.

The second special case happens when $\omega_c/\omega_h = \beta_h/\beta_c$. For the Otto cycle without the internal coupling, the heat absorbed from the hot bath is equal to the heat released to the

cold bath ($Q_h + Q_c = 0$), leading to zero work exchange $W = 0$. Consequently, the Otto cycle without coupling cannot function as a thermal machine in this case. However, after introducing the internal coupling, as in Eqs. (13)–(21), the energy flows become dependent on the coupling strength. By adjusting the internal coupling strength, inequivalent heat flows from different baths can occur, leading to work extraction or production.

Therefore, in both special cases, the presence of the internal coupling extends the operational regime of the quantum Otto cycle. In Secs. IV–V, we further analyze how the internal coupling influences the energy flows, operation regimes, and performance of various thermal machines, considering three types of limit cycles consisting of the Gibbs-state limit cycle (GSLC), the equilibrating limit cycle (ELC), and the non-equilibrating limit cycle (NELC). We assume that the interaction time in the adiabatic processes is always negligible and that the difference among these cycles is determined by the evolution time in the isochoric processes.

IV. Gibbs-State Limit Cycle

In this section, as shown in Fig. 1(a), we assume that the system quickly reaches equilibrium after starting interaction with heat baths and remains in thermal equilibrium during each isochoric process. The equilibrium state is defined as the Gibbs state, and hence we call it the Gibbs-state limit cycle (GSLC).

To determine the Gibbs state in each isochoric process, we diagonalize the system Hamiltonian, using the effective energy levels that incorporate the influence of the internal coupling strength. Although the effective basis in each process differs, we need to express all physical quantities in the entire Otto cycle in the original basis. Therefore, we switch from the original to the effective basis at each isochoric process to calculate the system state, and then

switch back from the effective to the original basis to calculate the physical quantities.

A. Formulation

To account for the internal coupling, we diagonalize the system Hamiltonian as follows:

$$\tilde{H}_S^\alpha = U_\alpha^\dagger H_S^\alpha U_\alpha = \begin{pmatrix} \epsilon_\alpha^- & 0 \\ 0 & \epsilon_\alpha^+ \end{pmatrix}, \quad (36)$$

where the eigenvalues are

$$\epsilon_\alpha^\pm = \frac{1}{2}(\omega_\alpha \pm \sqrt{4g_\alpha^2 + \omega_\alpha^2}), \quad (37)$$

and the corresponding eigenvectors are

$$|P_\alpha^+\rangle = \begin{pmatrix} \cos \theta_\alpha & \sin \theta_\alpha \end{pmatrix}^T, \quad (38)$$

$$|P_\alpha^-\rangle = \begin{pmatrix} -\sin \theta_\alpha & \cos \theta_\alpha \end{pmatrix}^T \quad (39)$$

with

$$\theta_\alpha = \arctan \frac{\epsilon_\alpha^+}{g_\alpha}. \quad (40)$$

The diagonalizing unitary transformation U_α in Eq. (36) is thus given by

$$U_\alpha = \begin{pmatrix} |P_\alpha^-\rangle & |P_\alpha^+\rangle \end{pmatrix}. \quad (41)$$

In the effective basis $|P_\alpha^\pm\rangle$ in each isochoric process $\alpha = h, c$, the Gibbs state is given by

$$\rho_{\text{Gibbs}}^\alpha = \frac{1}{Z_\alpha} (e^{-\beta_\alpha \epsilon_\alpha^+} |P_\alpha^+\rangle \langle P_\alpha^+| + e^{-\beta_\alpha \epsilon_\alpha^-} |P_\alpha^-\rangle \langle P_\alpha^-|), \quad (42)$$

where the inverse temperature $\beta_\alpha = 1/(kT_\alpha)$, and the partition function is

$$Z_\alpha = e^{-\beta_\alpha \epsilon_\alpha^-} + e^{-\beta_\alpha \epsilon_\alpha^+} = 2e^{-\frac{\beta_\alpha \omega_\alpha}{2}} \cosh \beta_\alpha \Delta_\alpha \quad (43)$$

with

$$\Delta_\alpha = \sqrt{g_\alpha^2 + \frac{\omega_\alpha^2}{2}}. \quad (44)$$

We put the Boltzmann constant k to unity hereafter.

Without the internal coupling, the efficiency and COP can be written in terms of the bare energy gaps ω_α . When the internal coupling g_α is introduced, such direct expressions are no longer valid because the effective Hamiltonians and the Gibbs states are defined in the diagonalizing eigenbases in Eqs. (38) and (39). To maintain consistency, we hereafter express all physical quantities in the original eigenbasis $\left(|g\rangle |e\rangle \right)$. The Gibbs state (42) is then expressed as

$$\rho_{\text{Gibbs}}^\alpha = \frac{1}{Z_\alpha} \left[e^{-\beta\epsilon_\alpha^+} \begin{pmatrix} \cos^2 \theta_\alpha & \cos \theta_\alpha \sin \theta_\alpha \\ \cos \theta_\alpha \sin \theta_\alpha & \sin^2 \theta_\alpha \end{pmatrix} + e^{-\beta\epsilon_\alpha^-} \begin{pmatrix} \sin^2 \theta_\alpha & -\cos \theta_\alpha \sin \theta_\alpha \\ -\cos \theta_\alpha \sin \theta_\alpha & \cos^2 \theta_\alpha \end{pmatrix} \right] \quad (45)$$

$$= \frac{1}{2\Delta_\alpha} \begin{pmatrix} 2\Delta_\alpha + \frac{\omega_\alpha \tanh \beta_\alpha \Delta_\alpha}{2} & -g_\alpha \tanh \beta_\alpha \Delta_\alpha \\ -g_\alpha \tanh \beta_\alpha \Delta_\alpha & 2\Delta_\alpha - \frac{\omega_\alpha \tanh \beta_\alpha \Delta_\alpha}{2} \end{pmatrix}. \quad (46)$$

As discussed in Sec. III, the internal coupling introduces off-diagonal coherence terms that modify the efficiency and COP. These terms can be represented by the function $f(g_\alpha, \beta_\alpha, \omega_\alpha)$ defined in Eq. (25), which depends on three parameters. For the Gibbs states (45), this function is specifically given by

$$f(g_\alpha, \beta_\alpha, \omega_\alpha) = -\frac{g_\alpha}{\Delta_\alpha} \tanh(\beta_\alpha \Delta_\alpha). \quad (47)$$

B. Numerical Results

1. Energy Flows

The heat absorptions and work extraction from the external environment to the internal system, as in Eqs. (13)–(21), can be rewritten as

$$Q_h = g_h [f(g_h, \beta_h, \omega_h) - f(g_c, \beta_c, \omega_c)] + \omega_h(\rho_{ee}^h - \rho_{ee}^c) \quad (48)$$

$$= \frac{(g_c g_h + \omega_c \omega_h / 4) \tanh \beta_c \Delta_c}{\Delta_c} - \Delta_h \tanh \beta_h \Delta_h, \quad (49)$$

$$Q_c = -g_c [f(g_h, \beta_h, \omega_h) - f(g_c, \beta_c, \omega_c)] - \omega_c(\rho_{ee}^h - \rho_{ee}^c) \quad (50)$$

$$= \frac{(g_c g_h + \omega_c \omega_h / 4) \tanh \beta_h \Delta_h}{\Delta_h} - \Delta_c \tanh \beta_c \Delta_c, \quad (51)$$

$$W = \frac{[g_c(g_c - g_h) + \omega_c(\omega_c - \omega_h)/4] \tanh \beta_c \Delta_c}{\Delta_c} + \frac{[g_h(g_h - g_c) + \omega_h(\omega_h - \omega_c)/4] \tanh \beta_h \Delta_h}{\Delta_h}. \quad (52)$$

The heat and work exchanges thus depend on six parameters: $\omega_h, \omega_c, g_h, g_c, \beta_h, \beta_c$. Without loss of generality, we can fix the energy unit to ω_c and the temperature unit to β_c , leaving four independent parameters.

In the standard Otto cycle without internal coupling, when $\omega_h/\omega_c = \beta_c/\beta_h$, the heat absorbed from the hot bath is equal to the heat released to the cold bath, leading to no work exchanges. Figure 4 represents the influence of the coupling strengths g_α on energy flows when $\omega_h/\omega_c = \beta_c/\beta_h$. The symbol P indicates areas of positive energy extraction, in which the internal system extracts energy from the external environment. In contrast, the symbol N indicates areas of negative energy extraction, in which the internal system releases energy to the external environment. The black boundaries between the P- and N-areas indicate the zero-energy flow.

We observe that, even under the condition $\omega_h/\omega_c = \beta_c/\beta_h = 1/5$, there are work ex-

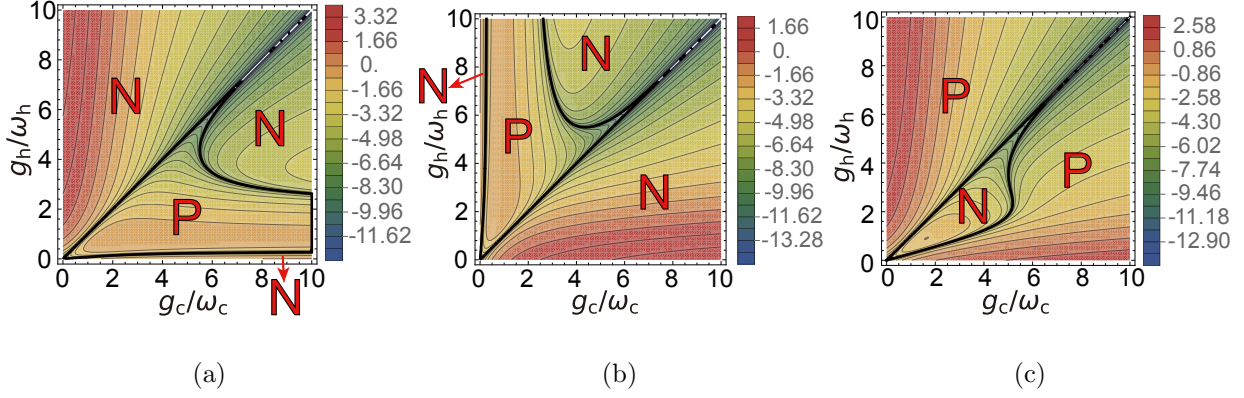


FIG. 4. Logarithmic plots of the energy flows (a) $\log|Q_h|$, (b) $\log|Q_c|$, and (c) $\log|W|$ depending on g_α/ω_α evaluated in the Gibbs-state limit cycle (GSLC). The black boundaries indicate the zero energy flow. The symbol P indicates the areas of the positive energy flow, in which the system absorbs energy from the environment. The symbol N indicates the areas of the negative energy flows, in which the system releases energy to the environment. We set the parameter values to $\omega_h = 5$, $\omega_c = 1$, $\beta_h = 0.2$, $\beta_c = 1$, and hence $\omega_h/\omega_c = \beta_c/\beta_h = 1/5$.

changes after introducing the internal coupling. The internal coupling strength influences the direction and amount of energy flow, leading to various types of thermal machines. First, as shown in Fig. 4(a), the internal system always releases heat to the hot bath when $g_h/\omega_h > g_c/\omega_c$. For $g_h/\omega_h < g_c/\omega_c$, varying g_h can reverse the direction of Q_h ; the system absorbs heat for small g_h but releases heat for large g_h . Next, as shown in Fig. 4(b), the internal system always releases heat to the cold bath when $g_h/\omega_h < g_c/\omega_c$. When $g_h/\omega_h > g_c/\omega_c$, increasing g_c reverses the direction of heat flow; the system absorbs heat for small g_c but releases heat for large g_c . Finally, Fig. 4(c) shows that the internal system always extracts work from the external work component when $g_h/\omega_h > g_c/\omega_c$. When $g_h/\omega_h < g_c/\omega_c$, near the boundary $g_h/\omega_h \approx g_c/\omega_c$ and for small coupling strengths g_α , the system can produce work to the environment, which represents the existence of an engine regime.

2. Operation Regimes

Based on the above analysis of the energy flows, we discover that the system can still operate as an engine or a refrigerator even under the condition $\omega_h/\omega_c = \beta_c/\beta_h$ after introducing the internal coupling. We identify the various operational modes of the Otto cycle from numerical analyses; only two modes can operate as a thermal machine. Note that we define the positive energy flows from the environment to the internal system.

Engine ($W < 0, Q_h > 0, Q_c < 0$): the internal system produces work to the work storage, absorbs heat from the hot bath, and releases heat to the cold bath, which is indicated by the green areas in Fig. 5.

Refrigerator ($W > 0, Q_h < 0, Q_c > 0$): the internal system extracts work from the work storage, releases heat to the hot bath, and absorbs heat from the cold bath, which is indicated by the blue area in Fig. 5.

Others: the Otto cycle cannot run as a thermal machine, which is indicated by the white areas in Fig. 5.

As shown in Fig. 5(a), for $\omega_c/\omega_c < \beta_c/\beta_h$ when the standard Otto cycle would work as an engine, increasing g_h can make the GSLC operate as a refrigerator instead. Conversely, as shown in Fig. 5(c), for $\omega_h/\omega_c > \beta_c/\beta_h$ when the standard Otto cycle would work as a refrigerator, we can control the coupling strengths g_α , so that the GSLC can operate as an engine.

In summary, by introducing and controlling the internal coupling, the operational regime of the quantum Otto cycle can be extended. The internal coupling thus enables the thermal cycle to exceed the conventional operational limits of both engines and refrigerators.

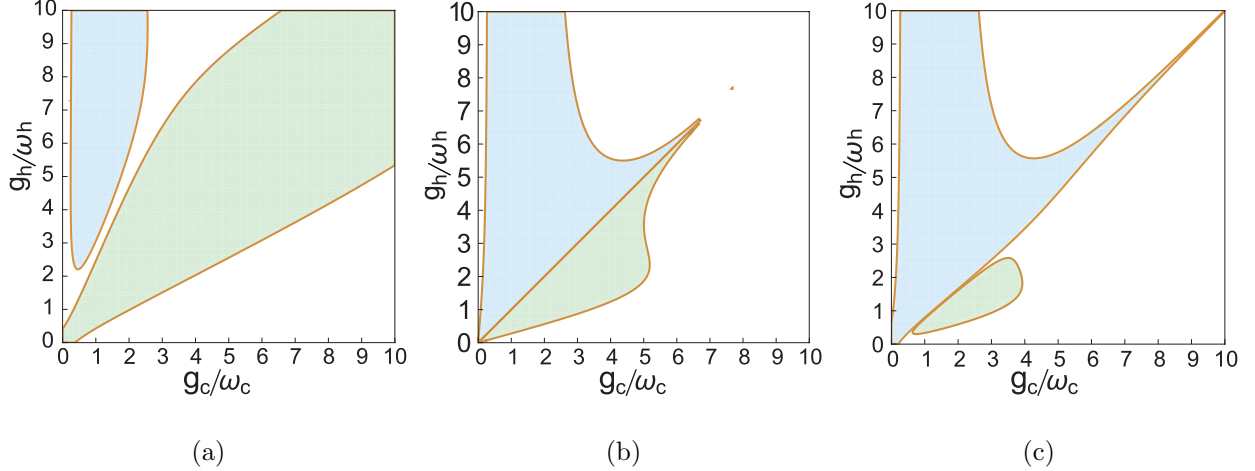


FIG. 5. Operation of the Otto cycle depending on the ratio g_α/ω_α ($\alpha = h, c$) in the Gibbs-state limit cycle (GSLC). In the blue areas on the left side of each figure, the Otto cycle operates as a refrigerator. In the green areas in the middle, the Otto cycle operates as an engine. In the white areas, the Otto cycle cannot run as a thermal machine. We set the energy ω_c and the inverse temperature β_c to unity, fix the inverse temperatures as $\beta_c/\beta_h = 5$, and increase the energy level ω_h from (a) to (c) as $\omega_h/\omega_c = 2, 5, 6$.

3. Efficiency and COP

We also analyze how internal coupling affects the Otto engine's efficiency and the refrigerator's coefficient of performance (COP) in the Gibbs-state limit cycle (GSLC). As shown in Fig. 5, although the internal coupling can shift the operation regime, the Otto cycle still mainly operates as an engine when $\omega_h/\omega_c < \beta_c/\beta_h$, while as a refrigerator when $\omega_h/\omega_c > \beta_c/\beta_h$.

For the comparison of the efficiency between the standard Otto cycle without coupling and the GSLC, we fix the inverse bath temperatures and the energy levels of the internal system as $\omega_h/\omega_c < \beta_c/\beta_h$ so that the GSLC can primarily function as an engine. As shown in Fig. 6(a), within the meshed region of (g_h, g_c) , the efficiency η_{cp} of the internal coupled system

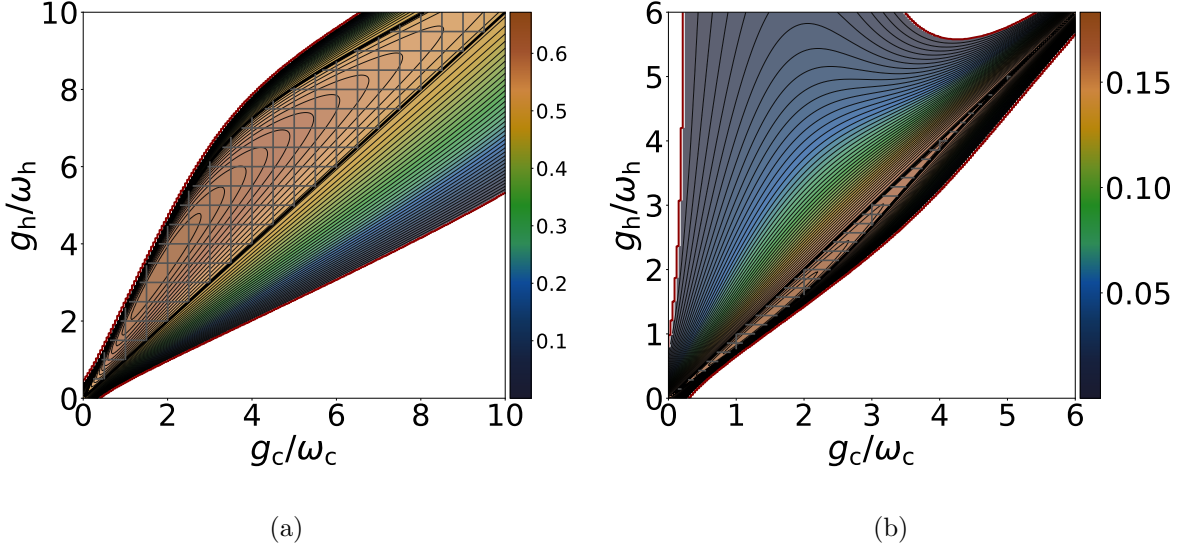


FIG. 6. Dependence of (a) efficiency η_{cp} of the Otto engine with $\omega_h = 2$ and (b) COP ξ_{cp} of the Otto cooler with $\omega_h = 7$ in the Gibbs-state limit cycle (GSLC) on the ratio g_α/ω_α . The black boundary indicates the efficiency η_{Otto} and COP ξ_{Otto} for the Otto cycle without the internal coupling. The meshing area indicates that the efficiency and the COP exceed the Otto limit with $\eta_{cp} > \eta_{Otto}$ and $\xi_{cp} > \xi_{Otto}$. We set the energy unit and temperature unit to $\omega_c = 1$ and $\beta_c = 1$, and the inverse temperature of the hot bath to $\beta_h = 0.2$.

exceeds the standard Otto efficiency without internal coupling at $(0,0)$. The efficiency η_{cp} increases as both of the coupling strengths g_α increase, reaches a maximum, and then decreases for larger values of g_α .

We can verify that the higher efficiency region always occurs for $g_h/\omega_h > g_c/\omega_c$. As summarized in Table I, after introducing internal coupling, a higher efficiency is obtained under the conditions

$$g_h/\omega_h > g_c/\omega_c \text{ and } f(g_h, \beta_h, \omega_h) < f(g_c, \beta_c, \omega_c),$$

with the operational constraints $W < 0$, $Q_c < 0$, and $Q_h > 0$. Under fixed temperatures and energy levels, the coupling strengths can thus be tuned to achieve the optimal efficiency.

Similarly, for the COP of the refrigerator, we fix the inverse bath temperature and the energy levels of the internal system as $\omega_h/\omega_c > \beta_c/\beta_h$ so that the GSLC can mainly operate as a refrigerator. As shown in Fig. 6(b), in the meshed area with proper sets of (g_h, g_c) , the COP is greater than the one plotted at the point $(0, 0)$, which is the COP without the coupling. By increasing the coupling strength, the COP initially increases and then decreases.

As shown in Fig. 6(b), following the illustration in Table II, after introducing the internal coupling, a higher COP is achieved under the conditions

$$f(g_h, \beta_h, \omega_h) > f(g_c, \beta_c, \omega_c) \text{ and } \frac{g_c}{\omega_c} > \frac{g_h - g_c}{\omega_h - \omega_c},$$

together with $Q_c > 0$, $Q_h < 0$, and $W > 0$. By adjusting the coupling strengths at fixed temperatures and energy levels, the quantum Otto refrigerator can thus achieve enhanced COP performance.

V. Open Quantum System under Markovian Approximation: ELC and NELC

In the previous section IV, we considered the case in which the system is thermalized to the Gibbs state promptly in each isochoric process and reaches the Gibbs-state limit cycle (GSLC). In this section, we analyze the Otto cycle as a Markovian dynamical open quantum system, and the isochoric processes (a) and (c) are described by the Gorini–Kossakowski–Sudarshan–Lindblad (GKSL) master equation [29, 34].

During the adiabatic processes (b) and (d) in Fig. 3, we assume the interaction time is negligible, so that the system Hamiltonian changes rapidly without altering the internal system state. During the isochoric processes (a) and (c), on the other hand, we consider the Markovian dynamical open quantum system, in which the non-equilibrium process is inevitable.

When the interaction time is short, the system cannot entirely equilibrate. As proven in Appendix A, the stroboscopic evolution over one Otto cycle defines a primitive, completely positive and trace-preserving (CPTP) map. According to the quantum Perron–Frobenius theorem, the dynamics finally converge to a unique periodic limit cycle. Within each cycle, if each isochoric process is short, the system alternates between two distinct states ρ_{NELC}^h and ρ_{NELC}^c , and the limit cycle is a non-equilibrating limit cycle (NELC), as illustrated in Fig. 1(c).

If we increase the interaction time to infinity in the isochoric processes, the limit cycle becomes an equilibrating limit cycle (ELC), as shown in Fig. 1(b). In the ELC, the state equilibrates in each isochoric process in the end, and should exhibit properties similar to those of the GSLC. In Appendix B, we derive the GKSL master equation using both local and global approaches. As detailed in Appendix B1, the local master equation is the standard GKSL master equation, which does not include the influence of the internal coupling. The equilibrium state (B14) derived from the local master equation is not the thermalized Gibbs state. On the other hand, as detailed in Appendix B2, the global master equation, which is updated to account for internal coupling, produces the correct equilibrium Gibbs state. Therefore, in the analysis, we utilize the global master equation rather than the local one.

A. Formulation

As proved in Appendix A, the Otto cycle converges to a periodic limit cycle after several cycles, alternating between two states, which can be expanded in the complete Liouvillian eigenbasis as

$$\tilde{\rho}_{\text{NELC}}^\alpha = \sum_i \tilde{c}_i^\alpha \tilde{\rho}_i^\alpha, \quad (53)$$

where $\tilde{\rho}_i^\alpha$ are the right eigenmatrices in Eqs. (B35)–(B38) of the global Liouvillian superoperator \mathcal{L}^α (B21), corresponding to the i th eigenvalue $\tilde{\lambda}_i$ in Eqs. (B27)–(B30), and \tilde{c}_i^α are the expansion coefficients. In each cycle, as shown in Fig. 1(c), the internal system changes from $\tilde{\rho}_{\text{NELC}}^{\text{h}}$ to $\tilde{\rho}_{\text{NELC}}^{\text{c}}$ in the isochoric process (a), and back from $\tilde{\rho}_{\text{NELC}}^{\text{c}}$ to $\tilde{\rho}_{\text{NELC}}^{\text{h}}$ in the isochoric process (c). The coefficients \tilde{c}_i^α are determined by the periodically steady condition in Eq. (A3).

As detailed in Appendix B2, the global master equation is derived in the diagonalizing basis of the system Hamiltonian. Hence, we perform several additional eigenbasis transformations to go back to the original basis of the Liouvillian superoperator \mathcal{L}^α (B21) in isochoric processes (a) and (c).

At the beginning of each isochoric process before calculating the evolution, we transform the system from the common basis

$$\begin{pmatrix} \rho_{\text{gg}}^\alpha & \rho_{\text{ge}}^\alpha \\ \rho_{\text{eg}}^\alpha & \rho_{\text{ee}}^\alpha \end{pmatrix}$$

to the diagonalizing basis

$$\begin{pmatrix} \tilde{\rho}_{\text{gg}}^\alpha & \tilde{\rho}_{\text{ge}}^\alpha \\ \tilde{\rho}_{\text{eg}}^\alpha & \tilde{\rho}_{\text{ee}}^\alpha \end{pmatrix}.$$

After each isochoric process, we transform the system back from the diagonalizing basis to the common basis. Therefore, following the periodically steady condition in Eq. (A3), the relation in Eqs. (A4) and (A5) between the states in different isochoric processes can be rewritten as

$$\tilde{\rho}_{\text{NELC}}^{\text{h}} = \sum_{i=0}^3 \text{Tr}[\tilde{\sigma}_i^{\text{h}} U_{\text{h}}^\dagger U_{\text{c}} \tilde{\rho}_{\text{NELC}}^{\text{c}} U_{\text{c}}^\dagger U_{\text{h}}] \tilde{\rho}_i^{\text{h}}, \quad (54)$$

$$\tilde{\rho}_{\text{NELC}}^{\text{c}} = \sum_{i=0}^3 \text{Tr}[\tilde{\sigma}_i^{\text{c}} U_{\text{c}}^\dagger U_{\text{h}} \tilde{\rho}_{\text{NELC}}^{\text{h}} U_{\text{h}}^\dagger U_{\text{c}}] \tilde{\rho}_i^{\text{c}}. \quad (55)$$

Note that the diagonalizing transformation in Eq. (41), the i th eigenvalue $\tilde{\lambda}_i^\alpha$ in Eqs. (B27)–(B30), and the left and right eigenmatrices $\tilde{\sigma}_i^\alpha$ and $\tilde{\rho}_i^\alpha$ in Eqs. (B31)–(B38) of the Liouvillian superoperator (B21), are controlled by the parameters $\{\beta_\alpha, \omega_\alpha, g_\alpha\}$ ($\alpha = \text{h, c}$).

Based on the periodically steady condition in Eqs. (54)–(55), the relations between the coefficients \tilde{c}_k^α are given by

$$\tilde{c}_k^{\text{h}} = \sum_{j=0}^3 \tilde{c}_j^{\text{c}} \text{Tr}[\tilde{\sigma}_k^{\text{h}} U_{\text{h}}^\dagger U_{\text{c}} \tilde{\rho}_j^{\text{c}} U_{\text{c}}^\dagger U_{\text{h}}] e^{\tilde{\lambda}_k^{\text{h}} t_{\text{h}}} \quad (56)$$

$$= \sum_{i=0}^3 \tilde{c}_i^{\text{h}} \sum_{j=0}^3 \text{Tr}[\tilde{\sigma}_j^{\text{c}} (U_{\text{c}}^\dagger U_{\text{h}} \tilde{\rho}_i^{\text{h}} U_{\text{h}}^\dagger U_{\text{c}})] \text{Tr}[\tilde{\sigma}_k^{\text{h}} (U_{\text{h}}^\dagger U_{\text{c}} \tilde{\rho}_j^{\text{c}} U_{\text{c}}^\dagger U_{\text{h}})] e^{\tilde{\lambda}_j^{\text{c}} t_{\text{c}}} e^{\tilde{\lambda}_k^{\text{h}} t_{\text{h}}}, \quad (57)$$

$$\tilde{c}_k^{\text{c}} = \sum_{j=0}^3 \tilde{c}_j^{\text{h}} \text{Tr}[\tilde{\sigma}_k^{\text{c}} U_{\text{c}}^\dagger U_{\text{h}} \tilde{\rho}_j^{\text{h}} U_{\text{h}}^\dagger U_{\text{c}}] e^{\tilde{\lambda}_k^{\text{c}} t_{\text{c}}} \quad (58)$$

$$= \sum_{i=0}^3 \tilde{c}_i^{\text{c}} \sum_{j=0}^3 \text{Tr}[\tilde{\sigma}_j^{\text{h}} (U_{\text{h}}^\dagger U_{\text{c}} \tilde{\rho}_i^{\text{c}} U_{\text{c}}^\dagger U_{\text{h}})] \text{Tr}[\tilde{\sigma}_k^{\text{c}} (U_{\text{c}}^\dagger U_{\text{h}} \tilde{\rho}_j^{\text{h}} U_{\text{h}}^\dagger U_{\text{c}})] e^{\tilde{\lambda}_j^{\text{h}} t_{\text{h}}} e^{\tilde{\lambda}_k^{\text{c}} t_{\text{c}}}. \quad (59)$$

Introducing the coefficient vector

$$\vec{c}^\alpha = \left(\tilde{c}_0^\alpha \quad \tilde{c}_1^\alpha \quad \tilde{c}_2^\alpha \quad \tilde{c}_3^\alpha \right)^T,$$

the above set of equations (56)–(59) can be written in a matrix form:

$$(\tilde{\mathbb{L}}_4 - \tilde{M}^\alpha) \vec{c}^\alpha = 0, \quad (60)$$

where the matrices \tilde{M}^α are defined by their k th row and i th column as

$$\tilde{M}_{k,i}^{\text{h}} = \sum_{j=0}^3 \text{Tr}[\tilde{\sigma}_j^{\text{c}} (U_{\text{c}}^\dagger U_{\text{h}} \tilde{\rho}_i^{\text{h}} U_{\text{h}}^\dagger U_{\text{c}})] \text{Tr}[\tilde{\sigma}_k^{\text{h}} (U_{\text{h}}^\dagger U_{\text{c}} \tilde{\rho}_j^{\text{c}} U_{\text{c}}^\dagger U_{\text{h}})] e^{\tilde{\lambda}_j^{\text{c}} t_{\text{c}}} e^{\tilde{\lambda}_k^{\text{h}} t_{\text{h}}}, \quad (61)$$

$$\tilde{M}_{k,i}^{\text{c}} = \sum_{j=0}^3 \text{Tr}[\tilde{\sigma}_j^{\text{h}} (U_{\text{h}}^\dagger U_{\text{c}} \tilde{\rho}_i^{\text{c}} U_{\text{c}}^\dagger U_{\text{h}})] \text{Tr}[\tilde{\sigma}_k^{\text{c}} (U_{\text{c}}^\dagger U_{\text{h}} \tilde{\rho}_j^{\text{h}} U_{\text{h}}^\dagger U_{\text{c}})] e^{\tilde{\lambda}_j^{\text{h}} t_{\text{h}}} e^{\tilde{\lambda}_k^{\text{c}} t_{\text{c}}}. \quad (62)$$

Since \tilde{M}^α represents a CPTP map, and there is only one zero-eigenvalue state $\tilde{\rho}_0^\alpha$, the NELC coefficients are uniquely determined. Therefore, we can determine the coefficients once the parameters $\{\beta_\alpha, \omega_\alpha, g_\alpha\}$ ($\alpha = \text{h, c}$) are fixed, yielding the NELC.

In Eqs. (13)–(21), the total energy flows during the isochoric processes are given by the system Hamiltonian and the states in the original basis. For the NELC, we can rewrite them as

$$Q_h = \text{Tr}[H_S^h(\rho_{\text{NELC}}^h - \rho_{\text{NELC}}^c)], \quad (63)$$

$$Q_c = \text{Tr}[H_S^c(\rho_{\text{NELC}}^c - \rho_{\text{NELC}}^h)]. \quad (64)$$

In each adiabatic process, the total work extracted from the environment during the adiabatic processes is given by

$$W_1 = \text{Tr}[(H_S^c - H_S^h)\rho_{\text{NELC}}^h], \quad (65)$$

$$W_2 = \text{Tr}[(H_S^h - H_S^c)\rho_{\text{NELC}}^c], \quad (66)$$

and the total work is given by

$$W = W_1 + W_2 = -(Q_h + Q_c), \quad (67)$$

which still obeys the second law of thermodynamics. Note that the relation between the system states in the original basis $\rho_{\text{NELC}}^\alpha$ and the diagonalized basis $\tilde{\rho}_{\text{NELC}}^\alpha$ of the Liouvillian (B21) is given by

$$\rho_{\text{NELC}}^\alpha = U_\alpha \tilde{\rho}_{\text{NELC}}^\alpha U_\alpha^\dagger. \quad (68)$$

In the limit of infinite interaction time, the system reaches equilibrium during each isochoric process, leading to an equilibrating limit cycle (ELC), as illustrated in Fig. 1(b), in which the influence of non-equilibrium terms becomes negligible after a long time. In each isochoric process of the ELC, the system state is the equilibrium steady state in the end, which is the zero-eigenvalue state $\tilde{\rho}_0^\alpha$ (B35) of the global Liouvillian (B21), corresponding to

the zero eigenvalue (B27):

$$\tilde{\rho}_{\text{ELC}}^{\alpha} = \tilde{\rho}_0^{\alpha} = \frac{1}{\tilde{\Gamma}_{\alpha}^{-} + \tilde{\Gamma}_{\alpha}^{+}} \begin{pmatrix} \tilde{\Gamma}_{\alpha}^{+} & 0 \\ 0 & \tilde{\Gamma}_{\alpha}^{-} \end{pmatrix}, \quad (69)$$

where the quantity $\tilde{\Gamma}_{\alpha}^{\pm}$ is defined in Eq. (B24). The relation between the system states in the original basis $\rho_{\text{ELC}}^{\alpha}$ and the diagonalized basis $\tilde{\rho}_{\text{ELC}}^{\alpha}$ of the Liouvillian (B21) is given by

$$\rho_{\text{ELC}}^{\alpha} = U_{\alpha} \tilde{\rho}_{\text{ELC}}^{\alpha} U_{\alpha}^{\dagger}. \quad (70)$$

Similarly, we can rewrite the total energy flows of the ELC as

$$Q_{\text{h}} = \text{Tr}[H_S^{\text{h}}(\rho_{\text{ELC}}^{\text{h}} - \rho_{\text{ELC}}^{\text{c}})], \quad (71)$$

$$Q_{\text{c}} = \text{Tr}[H_S^{\text{c}}(\rho_{\text{ELC}}^{\text{c}} - \rho_{\text{ELC}}^{\text{h}})]. \quad (72)$$

In each adiabatic process, the total work extracted from the environment is given by

$$W_1 = \text{Tr}[(H_S^{\text{c}} - H_S^{\text{h}})\rho_{\text{ELC}}^{\text{h}}], \quad (73)$$

$$W_2 = \text{Tr}[(H_S^{\text{h}} - H_S^{\text{c}})\rho_{\text{ELC}}^{\text{c}}], \quad (74)$$

which still obeys the second law of thermodynamics (67).

B. Numerical Results: From NELC to ELC

In this section, by adjusting the interaction time, we observe the convergence from the non-equilibrating limit cycle (NELC) to the equilibrating limit cycle (ELC), compare the NELC, the ELC, and the Gibbs-state limit cycle (GSLC), and examine the influence of the coupling strength and the interaction time on the operation regimes and the performances of the NELC. We utilize the global approach of the GKSL master equation, as detailed in Appendix B.

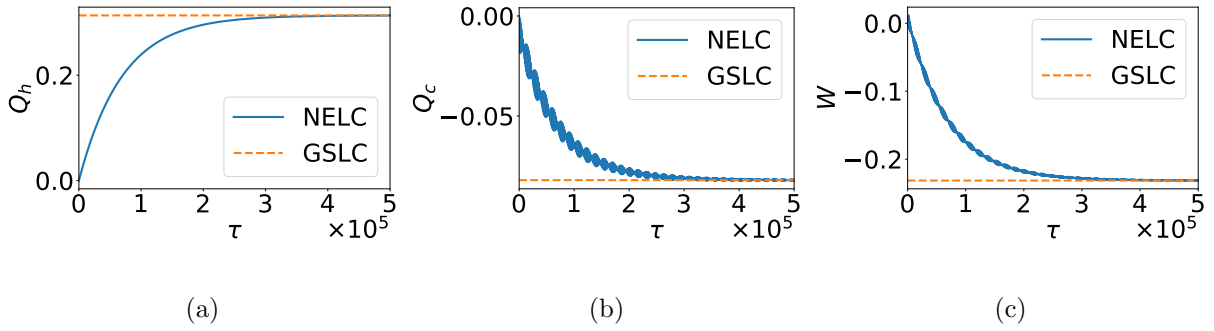


FIG. 7. Time dependence of the energy flows (a) Q_h , (b) Q_c , and (c) W . The blue solid lines indicate the non-equilibrating limit cycle (NELC) derived from the global GKSL master equation, while the red dashed lines indicate the Gibbs-state limit cycle (GSLC). We set the parameter values to $\omega_c = 1$, $\omega_h = 5$, $\beta_c = 1$, $\beta_h = 0.2$, $g_c = 1$, $g_h = 4$.

Firstly, we fix all the other parameters $\{\omega_\alpha, \beta_\alpha, g_\alpha\}$ and examine the dynamics from the non-equilibrating limit cycle (NELC) to the equilibrating limit cycle (ELC) by only adjusting the interaction time $\tau = t_h = t_c$. If the NELC operates as an engine, the power is given by

$$P = \frac{W}{t_h + t_c} = \frac{W}{2\tau}. \quad (75)$$

Following Sec. III A, the heat flows Q_α are defined in Eqs. (13)–(15) and the works are defined in Eqs. (17)–(21). When the limit cycle runs as an engine that $Q_h > 0$, $Q_c < 0$, $W < 0$, the efficiency is defined in Eq. (22). When the limit cycle runs as a refrigerator that $Q_h < 0$, $Q_c > 0$, $W > 0$, the coefficient of performance (COP) is defined in Eq. (26).

As shown in Fig. 7, when the interaction time is zero, there is no heat flow Q_α in each isochoric process, and no work W in the adiabatic processes. As interaction time increases, the NELC approaches the ELC. The ELC derived from the global master equation exhibits the same properties as the Gibbs-state limit cycle (GSLC), confirming the validity of the global GKSL master equation.

Unlike the GSLC, in which we did not consider the interaction time, the NELC with a

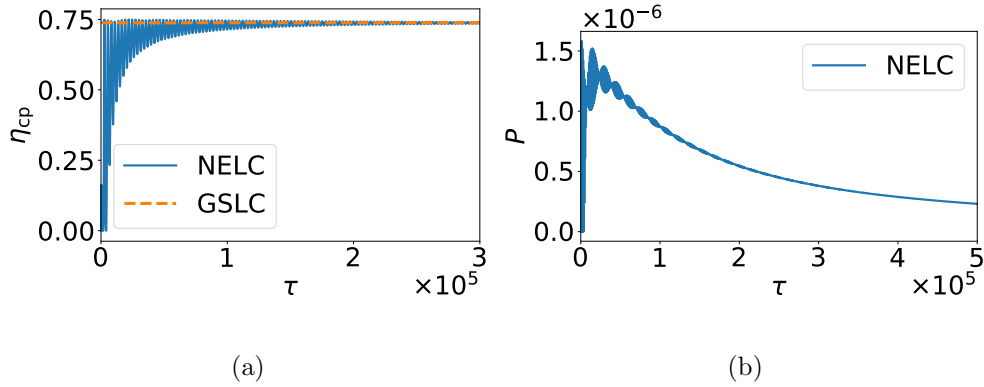


FIG. 8. Time dependence of (a) the efficiency η_{cp} and (b) the power P . The blue solid lines indicate the non-equilibrating limit cycle (NELC) derived from the global GKSL master equation. In (a), the red dashed line indicates the Gibbs-state limit cycle (GSLC). The GSLC neglects the influence of interaction time, leading to no power. In the ELC, due to the infinite interaction time, the power is zero too. The power of the NELC is defined in Eq. (75). We set the parameter values to $\omega_c = 1$, $\omega_h = 5$, $\beta_c = 1$, $\beta_h = 0.2$, $g_c = 1$, $g_h = 4$.

non-zero, finite interaction time has a finite power (75). Following the operation regime of GSLC in Fig. 5, we fix the parameters so that the ELC operates as an engine. As shown in Fig. 8, both efficiency and power are zero when the interaction time is zero, because of no interaction between the internal system and the external heat baths. When the interaction time is non-zero, increasing it decreases the power while increasing the efficiency. When the interaction time is large and approaches infinity, the efficiency converges to the equilibrium and maximum, while the power approaches zero.

For a better understanding of the influence of the coupling strength on the operation regime and performances in NELC, we adjust the coupling strengths g_α and fix the interaction duration $t_h = t_c = \tau$ to three representative values ($\tau = 10^2$, 10^4 , and 10^6). As shown in Figs. 7 and 8, strong oscillations in the numerical results are inevitable for short interaction

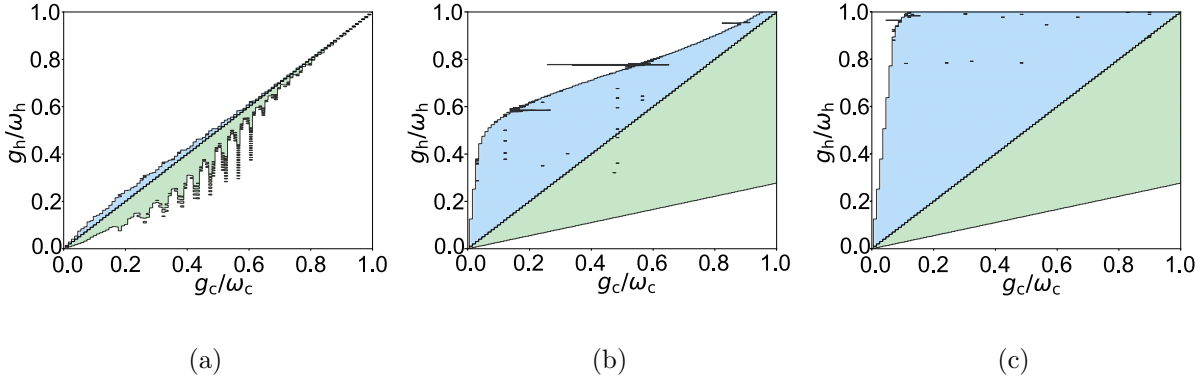


FIG. 9. Operation of the Otto cycle depending on the coupling strengths g_α ($\alpha = h, c$) of NELC derived from the global master equation with interaction time (a) $\tau = 10^2$, (b) $\tau = 10^4$, and (c) $\tau = 10^6$. In the blue area on the left side of the figure, the Otto cycle operates as a refrigerator. In the green area in the middle of the figure, the Otto cycle operates as an engine. In the white area, the system cannot run as a thermal machine. Same as in Fig. 5(a), we set the parameter values to $\omega_c = 1$, $\omega_h = 5$, $\beta_c = 1$, $\beta_h = 0.2$

times. In the latter discussion, to avoid strong oscillations in the original data, we compute time-averaged values for each quantity, yielding physically interpretable results.

For the operation regime, we focus on the specific condition $\beta_c/\beta_h = \omega_h/\omega_c$, under which the Otto cycle cannot operate as a thermal machine in the absence of internal coupling. For comparison between the NELC and the GSLC, which should exhibit the same properties as the ELC, we set the other parameters $\{\omega_\alpha, \beta_\alpha\}$ ($\alpha = h, c$) to be the same as in Fig. 5(a).

As shown in Fig. 9, under the condition $\beta_c/\beta_h = \omega_h/\omega_c$, all the NELCs act as an engine when $g_h/\omega_h < g_c/\omega_c$, and as a refrigerator when $g_h/\omega_h > g_c/\omega_c$, which is consistent with the GSLC and ELC shown in Fig. 5(a). However, compared to the operation regime of GSLC and ELC, the thermal-machine regime in Fig. 9 of NELC is narrower, making it more difficult for the Otto cycle to operate as a thermal machine. When we increase the interaction time,

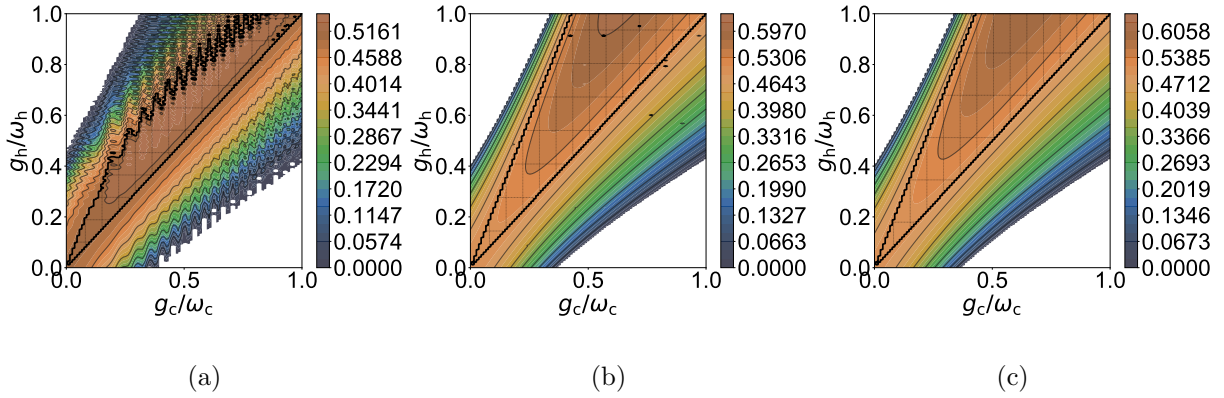


FIG. 10. Efficiency of the Otto engine depending on the coupling strengths g_α ($\alpha = h, c$) of NELC derived from the global master equation with interaction time (a) $\tau = 10^2$, (b) $\tau = 10^4$, and (c) $\tau = 10^6$. Same as in Figs. 6(a), we set the parameters values to $\omega_c = 1$, $\omega_h = 2$, $\beta_c = 1$, $\beta_h = 0.2$

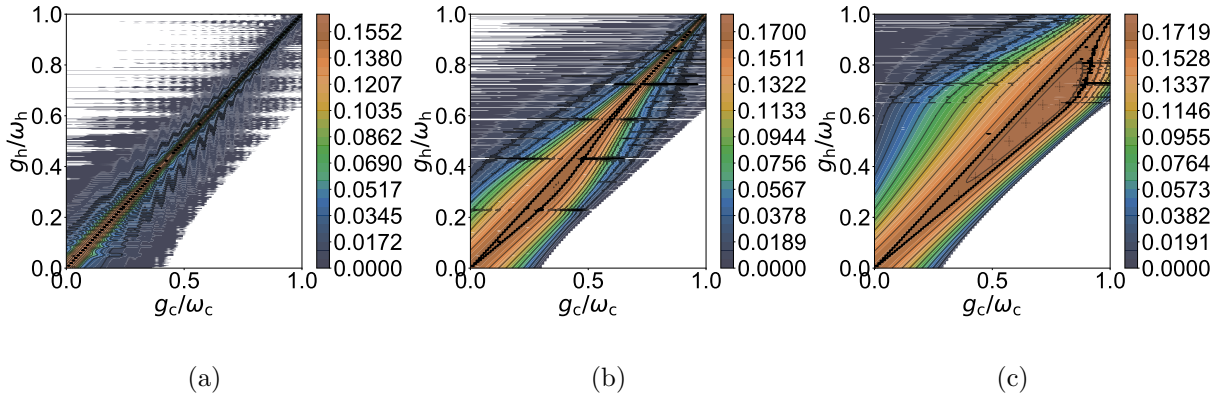


FIG. 11. COP of the Otto refrigerator depending on the coupling strengths g_α ($\alpha = h, c$) of NELC derived from the global master equation with interaction time (a) $\tau = 10^2$, (b) $\tau = 10^4$, and (c) $\tau = 10^6$. Same as in as in Figs. 6(b), we set the parameters values to $\omega_c = 1$, $\omega_h = 7$, $\beta_c = 1$, $\beta_h = 0.2$

the region of the thermal-machine operations expands and gradually converges to the ELC case in Fig. 5(a).

The efficiency and COP at NELC, as shown in Figs. 10–11, are both affected by the

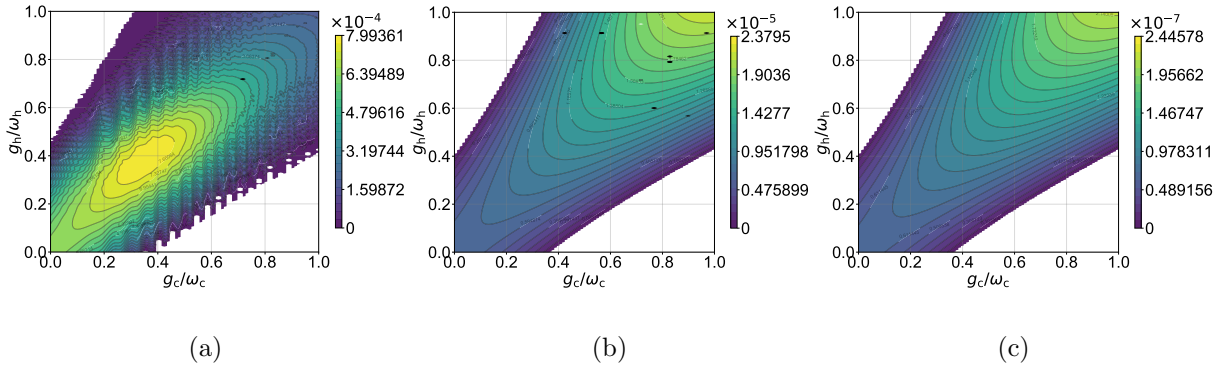


FIG. 12. Power of the Otto engine depending on the coupling strengths g_α ($\alpha = h, c$) of NELC derived from the global master equation with interaction time (a) $\tau = 10^2$, (b) $\tau = 10^4$, and (c) $\tau = 10^6$. Parameters: $\omega_c = 1$, $\omega_h = 2$, $\beta_c = 1$, $\beta_h = 0.2$

coupling strength. As with the system at ELC, as shown in Fig. 6, the internal coupling can improve performance. However, the efficiency and COP of NELC are both smaller and lower than those of GSLC and ELC. This is consistent with the reduced degree of thermalization in the nonequilibrium regime.

On the other hand, the output power, as shown in Fig. 12 is higher in NELC than in ELC, consistent with the universal power-efficiency trade-off [32, 33] in Fig. 8. For very short interaction times, the power increases rapidly as the interaction time τ increases, due to the enhanced energy exchange. However, if we increase the interaction time τ , the power decreases because the cycle duration increases faster than the corresponding energy gain. When the system approaches ELC from NELC, the power decreases and approaches zero.

In summary, both the performance and the operational regime of the Otto cycle are strongly affected by both the coupling strength and the interaction time. When we increase the interaction time, the system evolves from a highly oscillated NELC toward the ELC, leading to a broader thermal-machine regime and higher efficiency and COP. However, the power output shows the opposite trend; it first increases in ultra-short interaction time and

then decreases, reflecting the trade-off between power and efficiency [32, 33]. These results clarify how the interaction time mediates the transition from NELC to ELC, bridging non-equilibrium dynamics and steady-state thermodynamics.

VI. Conclusion

In the work, we extend the quantum Otto cycle to a more general case by considering the influence of the internal coupling. The internal coupling can produce off-diagonal coherence, and hence affect the performance and the operation.

On one hand, as in Tables I and II, we conclude the influence of the coupling strength on efficiency and COP, respectively. Compared to the quantum Otto cycle without internal coupling described in Sec. II, we demonstrate the influence of the internal coupling on the engine's efficiency and the refrigerator's COP. With internal couplings, not only can better performance exceeding the Otto bound be achieved, but the operating regime can also be shifted.

On the other hand, we clarify three cases from equilibrium to non-equilibrium cycles, consisting of the Gibbs-state limit cycle (GSLC) without considering the interaction time, equilibrating limit cycle (ELC) with infinite interaction time, and non-equilibrating limit cycle (NELC) with short interaction time, and analyze the influence of internal coupling on both equilibrium and non-equilibrium Otto cycles.

For GSLC in Sec. IV, we numerically analyze the influence of the coupling strength on energy flows, efficiency, and COP in each isochoric process. The numerical results demonstrate the properties of a thermal-equilibrium Otto cycle with internal coupling, confirm the results in Tables I and II, and provide the range of coupling strengths for achieving higher efficiency or COP.

Considering the interaction time in each isochoric process within the Markovian approximation, we analyze its influence on NELC and demonstrate convergence from NELC to ELC. In Appendix A, with a short interaction time, we confirm that the Otto cycle converges to a steady cycle, yielding NELC. In Appendix B, we clarify the difference between the local and global GKSL master equations, and validate the global one in the internal coupled quantum Otto cycle. In Sec. V, by adjusting the interaction time, we demonstrate the convergence from the NELC to the ELC, which exhibits the same properties as the GSLC, and examine the influence of the internal coupling on the NELC with different interaction times. For a shorter interaction time, the efficiency and the COP are lower, and the thermal-machine regime is narrower, but the power is higher. Inversely, the power decreases, while the efficiency (COP) and thermal-machine regime become broader as the interaction time increases, obeying the trade-off law between efficiency and power [32, 33].

VII. Acknowledgment

This work acknowledges financial support from the WINGS-QSTEP program of the University of Tokyo.

A. Existence and convergence to a Floquet non-equilibrium steady state

Rather than focusing on the continuous-time dynamics within each stroke, it is convenient to describe the evolution stroboscopically. Let ρ_n denote the system state at the beginning of the n th cycle. The evolution over one complete Otto cycle can be written as a discrete map

$$\rho_{n+1} = \mathcal{M}(\rho_n), \tag{A1}$$

where the one-cycle map is given by

$$\mathcal{M} = \mathcal{E}_c \circ U_c \circ \mathcal{E}_h \circ U_h. \quad (\text{A2})$$

Here, $U_\alpha(\rho) = U_\alpha \rho U_\alpha^\dagger$ denotes the unitary evolution during the isochoric processes, while \mathcal{E}_α represents the quantum channel generated by the global GKSL master equation during the hot (cold) isochoric stroke over a finite interaction time.

Each component of the cycle map \mathcal{M} is completely positive and trace preserving (CPTP). Consequently, their concatenation \mathcal{M} is also a CPTP map acting on a finite-dimensional Hilbert space. Moreover, due to the presence of finite system-bath coupling and internal coupling during the isochoric strokes, population transfer between all relevant energy eigenstates is allowed, and no nontrivial invariant subspace is preserved. As a result, the one-cycle map \mathcal{M} is primitive.

According to the quantum Perron–Frobenius theorem, a primitive CPTP map admits a unique fixed point ρ^* , corresponding to an eigenvalue $\lambda = 1$, while all other eigenvalues satisfy $|\lambda_i| < 1$. Therefore, for any initial state ρ_0 ,

$$\lim_{n \rightarrow \infty} \mathcal{M}^n(\rho_0) = \rho^* = \rho_{\text{NELC}}^c. \quad (\text{A3})$$

This fixed point ρ^* comprises a non-equilibrium limit cycle (NELC) of the Otto engine.

It is important to emphasize that the NELC does not correspond to a time-independent stationary state. Instead, it represents a periodic steady-state trajectory within each cycle.

In particular, the states associated with different strokes in the NELC are given by

$$\rho_{\text{NELC}}^h = \mathcal{E}_h \circ U_h(\rho^*) = \mathcal{E}_h \circ U_h(\rho_{\text{NELC}}^c), \quad (\text{A4})$$

$$\rho_{\text{NELC}}^c = \mathcal{E}_c \circ U_c(\rho_{\text{NELC}}^h). \quad (\text{A5})$$

In Sec. V A, these equations are rewritten as in Eqs. (54) and (55). In general, these two

states are distinct:

$$\rho_{\text{NELC}}^{\text{h}} \neq \rho_{\text{NELC}}^{\text{c}}. \quad (\text{A6})$$

The system thus converges to a unique periodic orbit rather than a single static state, enabling sustained energy exchange with the hot and cold reservoirs.

B. Comparison Between Local and Global Master Equations

In the isochoric processes of the quantum Otto cycle, we utilize the Gorini–Kossakowski–Sudarshan–Lindblad (GKSL) master equation to describe the Markovian quantum open system. The standard approach of the GKSL master equation neglects the influence of the internal coupling, which is called the local master equation. Considering the influence of internal coupling, the GKSL master equation is updated using a global approach, yielding the global master equation [24, 29–31].

1. Local Master Equation

For comparison, we briefly summarize the formulation of the local master equation, in which the internal coupling is not incorporated into the dissipative part. The system dynamics is governed by the standard GKSL form

$$\dot{\rho}_{\alpha}(t) = -i[H_S^{\alpha}, \rho_{\alpha}] + \gamma_{\alpha}^{+} \mathcal{D}(\sigma_S^{-}) + \gamma_{\alpha}^{-} \mathcal{D}(\sigma_S^{+}), \quad (\text{B1})$$

with the dissipator

$$\mathcal{D}(\hat{O}) = \hat{O}\rho\hat{O}^{\dagger} - \frac{1}{2}\{\hat{O}^{\dagger}\hat{O}, \rho\}, \quad (\text{B2})$$

the system Hamiltonian H_S^{α} as in Eq. (12), the Pauli matrices σ_S^{\pm} , and the dissipation rate γ_{α}^{\pm} .

We set the dissipation rates to

$$\gamma_\alpha^\pm = \gamma(\pm\omega_\alpha, \beta_\alpha), \quad (\text{B3})$$

with the bath correlation function

$$\gamma(\omega, \beta) = \begin{cases} J(\omega) n(\beta, \omega), & \omega < 0, \\ J(\omega) [n(\beta, \omega) + 1], & \omega > 0, \end{cases} \quad (\text{B4})$$

with $J(\omega)$ being the spectral density and $n(\beta, \omega)$ the Bose-Einstein distribution:

$$J(\omega) = \Gamma\omega e^{-\omega^s/\omega_{ct}^{1-s}}, \quad (\text{B5})$$

$$n(\beta, \omega) = \frac{1}{e^{\beta\omega} - 1}, \quad (\text{B6})$$

where ω_{ct} is the cut-off frequency and Γ indicates the coupling strength of the spectral density. The exponent s characterizes the low-frequency behavior of the bath spectral density and determines whether the environment is sub-Ohmic ($s < 1$), Ohmic ($s = 1$), or super-Ohmic ($s > 1$). In the analysis of the Markovian dynamical system in Sec. V, we assume an Ohmic environment and set $s = 1$.

Flattening the density matrix ρ_α into a vector $|\psi_\alpha\rangle = (\rho_{gg}^\alpha, \rho_{ge}^\alpha, \rho_{eg}^\alpha, \rho_{ee}^\alpha)^T$, we can write the master equation in terms of a 4×4 Liouvillian superoperator:

$$\frac{d}{dt} |\psi_\alpha(t)\rangle = \mathcal{L}_\alpha |\psi_\alpha(t)\rangle, \quad (\text{B7})$$

with

$$\mathcal{L}_\alpha = \begin{pmatrix} -\gamma_\alpha^- & ig_\alpha & -ig_\alpha & \gamma_\alpha^+ \\ ig_\alpha & -\frac{1}{2}(\gamma_\alpha^+ + \gamma_\alpha^- - 2i\omega_\alpha) & 0 & -ig_\alpha \\ -ig_\alpha & 0 & -\frac{1}{2}(\gamma_\alpha^+ + \gamma_\alpha^- + 2i\omega_\alpha) & ig_\alpha \\ \gamma_\alpha^- & -ig_\alpha & ig_\alpha & -\gamma_\alpha^+ \end{pmatrix}. \quad (\text{B8})$$

The spectral properties of \mathcal{L}_α can be obtained analytically. In particular, the Liouvillian admits a unique zero eigenvalue λ_0^α corresponding to a stationary state. The remaining eigenvalues $\lambda_{i=1,2,3}^\alpha$ have negative real parts, ensuring relaxation toward this steady state, given by the three roots of the cubic equation:

$$F_3(\lambda) = 8g^2(\gamma_\alpha^- + \gamma_\alpha^+ + 2\lambda) + (\gamma_\alpha^- + \gamma_\alpha^+ + \lambda)(\gamma_\alpha^{-2} + \gamma_\alpha^{+2} + 4\gamma_\alpha^+\lambda + 2\gamma_\alpha^-(\gamma_\alpha^+ + 2\lambda) + 4(\lambda^2 + \omega_\alpha^2)) \quad (\text{B9})$$

Corresponding to the i th eigenvalue λ_i^α , the left eigenvectors

$$\begin{pmatrix} \rho_{gg}^\alpha & \rho_{ge}^\alpha & \rho_{eg}^\alpha & \rho_{ee}^\alpha \end{pmatrix} \quad (\text{B10})$$

and the right eigenvectors

$$\begin{pmatrix} \rho_{gg}^\alpha & \rho_{ge}^\alpha & \rho_{eg}^\alpha & \rho_{ee}^\alpha \end{pmatrix}^T \quad (\text{B11})$$

are bi-orthogonal to each other.

The left eigenvectors corresponding to i th eigenvalue λ_i^α are given by

$$\langle L_0^\alpha | = \begin{pmatrix} 1 & 0 & 0 & 1 \end{pmatrix}, \quad (\text{B12})$$

$$\langle L_j^\alpha | = \begin{pmatrix} \frac{\gamma_\alpha^- - \gamma_\alpha^+ + \lambda_j^\alpha}{\gamma_\alpha^- - \gamma_\alpha^+ - \lambda_j^\alpha} \\ -\frac{i(2\lambda_j^\alpha)(8g_\alpha^2 + 2(\gamma_\alpha^- + \gamma_\alpha^+)(\gamma_\alpha^- + \gamma_\alpha^+ - 2i\omega_\alpha) + (3\gamma_\alpha^- + 3\gamma_\alpha^+ - 2i\omega_\alpha)(2*\lambda_j^\alpha) + (2\lambda_j^\alpha)^2)}{2g_\alpha(-2\gamma_\alpha^- + 2\gamma_\alpha^+ + (2\lambda_j^\alpha))(\gamma_\alpha^- + \gamma_\alpha^+ - 2i\omega_\alpha + (2\lambda_j^\alpha))} \\ -\frac{4ig_\alpha(2\lambda_j^\alpha)}{(-2\gamma_\alpha^- + 2\gamma_\alpha^+ + (2\lambda_j^\alpha))(\gamma_\alpha^- + \gamma_\alpha^+ - 2i\omega_\alpha + (2*\lambda_j^\alpha))} \\ 1 \end{pmatrix}^T. \quad (\text{B13})$$

The right eigenvectors are

$$|R_0^\alpha\rangle = \frac{1}{N_0^\alpha} \begin{pmatrix} 4g_\alpha^2(\gamma_\alpha^- + \gamma_\alpha^+) + \gamma_\alpha^-(\gamma_\alpha^{-2} + 2\gamma_\alpha^-\gamma_\alpha^+ + \gamma_\alpha^{+2} + 4\omega_\alpha^2) \\ 2ig(\gamma_\alpha^- - \gamma_\alpha^+)(\gamma_\alpha^- + \gamma_\alpha^+ + 2i\omega_\alpha) \\ -2ig(\gamma_\alpha^- - \gamma_\alpha^+)(\gamma_\alpha^- + \gamma_\alpha^+ - 2i\omega_\alpha) \\ 4g_\alpha^2(\gamma_\alpha^- + \gamma_\alpha^+) + \gamma_\alpha^+(\gamma_\alpha^{-2} + 2\gamma_\alpha^-\gamma_\alpha^+ + \gamma_\alpha^{+2} + 4\omega_\alpha^2) \end{pmatrix}, \quad (\text{B14})$$

$$|R_j^\alpha\rangle = \frac{1}{N_j^\alpha} \begin{pmatrix} g_\alpha^2(\gamma_\alpha^- - \gamma_\alpha^+ - \lambda_j^\alpha)(\gamma_\alpha^- + \gamma_\alpha^+ + 2\lambda_j^\alpha - 2i\omega_\alpha)(\gamma_\alpha^- + \gamma_\alpha^+ + 2\lambda_j^\alpha + 2i\omega_\alpha) \\ -(ig(\gamma_\alpha^- - \gamma_\alpha^+ - \lambda_j^\alpha)(4g_\alpha^2 + (\gamma_\alpha^- + \gamma_\alpha^+ + \lambda_j^\alpha)(\gamma_\alpha^- + \gamma_\alpha^+ + 2\lambda_j^\alpha + 2i\omega_\alpha))(\gamma_\alpha^- + \gamma_\alpha^+ + 2\lambda_j^\alpha - 2i\omega_\alpha)) \\ -(4ig^3(\gamma_\alpha^- - \gamma_\alpha^+ - \lambda_j^\alpha)(\gamma_\alpha^- + \gamma_\alpha^+ + 2\lambda_j^\alpha - 2i\omega_\alpha)) \\ -(g_\alpha^2(\gamma_\alpha^- - \gamma_\alpha^+ - \lambda_j^\alpha)(\gamma_\alpha^- + \gamma_\alpha^+ + 2\lambda_j^\alpha - 2i\omega_\alpha)(\gamma_\alpha^- + \gamma_\alpha^+ + 2\lambda_j^\alpha + 2i\omega_\alpha)) \end{pmatrix} \quad (\text{B15})$$

where

$$N_0^\alpha = (\gamma_\alpha^- + \gamma_\alpha^+)(8g_\alpha^2 + \gamma_\alpha^{-2} + 2\gamma_\alpha^-\gamma_\alpha^+ + \gamma_\alpha^{+2} + 4\omega_\alpha^2), \quad (\text{B16})$$

$$N_j^\alpha = \lambda_j^\alpha(32g_\alpha^4 + (\gamma_\alpha^- + \gamma_\alpha^+ + \lambda_j^\alpha)^2(\gamma_\alpha^{-2} + \gamma_\alpha^{+2} + 4\gamma_\alpha^+\lambda_j^\alpha + 2\gamma_\alpha^-(\gamma_\alpha^+ + 2\lambda_j^\alpha) + 4(\lambda_j^{\alpha 2} + \omega_\alpha^2)) \\ + 2g_\alpha^2(5\gamma_\alpha^{-2} + 5\gamma_\alpha^{+2} + 16\gamma_\alpha^+\lambda_j^\alpha + 2\gamma_\alpha^-(5\gamma_\alpha^+ + 8\lambda_j^\alpha) + 4(3\lambda_j^{\alpha 2} + \omega_\alpha^2))) \quad (\text{B17})$$

The right eigenvector $|R_0^\alpha\rangle$ is the equilibrium state, corresponding to the zero eigenvalue λ_0^α of the local Liouvillian superoperator \mathcal{L}_α . Due to the neglect of internal coupling in the construction of the dissipator, it does not correspond to the Gibbs state of the interacting system Hamiltonian. The local master equation yields a thermodynamically inconsistent limit cycle in the presence of internal coupling and is therefore invalid in our model.

2. Global Master Equation

Similar to the derivation of the global master equation in the multi-qubit system [24, 29–31], to generalize the local master equation to the global one in our single-qubit system, we rewrite the interaction Hamiltonian in the diagonalized basis:

$$\tilde{H}_I^\alpha(t) = e^{i\tilde{H}_S^\alpha t} U_\alpha^\dagger H_I U_\alpha e^{-i\tilde{H}_S^\alpha t} \quad (\text{B18})$$

$$= e^{i\tilde{H}_S^\alpha t} (U_\alpha^\dagger \sigma_S^x U_\alpha) e^{-i\tilde{H}_S^\alpha t} \sum_{k,\alpha} (V_{k,\alpha} \hat{b}_\alpha + V_{k,\alpha}^* \hat{b}_\alpha^\dagger) \quad (\text{B19})$$

$$= (-\sin(2\theta) \tilde{\sigma}_S^z + \cos(2\theta) e^{-i\tilde{\omega}_\alpha t} \tilde{\sigma}_S^+ + \cos(2\theta) e^{i\tilde{\omega}_\alpha t} \tilde{\sigma}_S^-) \sum_{k,\alpha} (V_{k,\alpha} \hat{b}_\alpha + V_{k,\alpha}^* \hat{b}_\alpha^\dagger), \quad (\text{B20})$$

where $\tilde{\omega}_\alpha = \epsilon_\alpha^+ - \epsilon_\alpha^- = \sqrt{4g_\alpha^2 + \omega_\alpha^2}$. The angle θ , the diagonalized system Hamiltonian, and the diagonalizing transformation U_α are defined in Eqs. (40), (36) and (41), respectively.

The Pauli matrices in the diagonalized map are $\tilde{\sigma}_S^z$ and $\tilde{\sigma}_S^\pm$.

In deriving the GKSL master equation, the system operators are decomposed into their Fourier components, and the bath spectral density assigns a weight to each transition frequency:

$$\frac{d\tilde{\rho}_\alpha}{dt} = \tilde{\mathcal{L}}_\alpha \tilde{\rho}_\alpha = -i[\tilde{H}_S^\alpha, \tilde{\rho}_\alpha] + \tilde{\gamma}_\alpha^+ \mathcal{D}(\cos(2\theta) \tilde{\sigma}_S^+) + \tilde{\gamma}_\alpha^- \mathcal{D}(\cos(2\theta) \tilde{\sigma}_S^-) + \tilde{\gamma}_\alpha(0) \mathcal{D}(-\sin(2\theta) \tilde{\sigma}_S^z). \quad (\text{B21})$$

Under the diagonalized system basis

$$\tilde{\rho}_\alpha = \begin{pmatrix} \tilde{\rho}_{\text{gg}}^\alpha & \tilde{\rho}_{\text{ge}}^\alpha \\ \tilde{\rho}_{\text{eg}}^\alpha & \tilde{\rho}_{\text{ee}}^\alpha \end{pmatrix},$$

as in Eq. (36), there is no energy gap for the transition

$$\tilde{\sigma}_S^z = \begin{pmatrix} 1 & 0 \\ 0 & -1 \end{pmatrix},$$

while the excitation frequency $\Delta\omega = \tilde{\omega}_\alpha$ is associated with

$$\tilde{\sigma}_S^+ = \begin{pmatrix} 0 & 1 \\ 0 & 0 \end{pmatrix},$$

and the de-excitation frequency $\Delta\omega = -\tilde{\omega}_\alpha$ is associated with

$$\tilde{\sigma}_S^- = \begin{pmatrix} 0 & 0 \\ 1 & 0 \end{pmatrix}.$$

Assuming the Ohmic spectral density $J(\omega) \propto \omega$, we have $\tilde{\gamma}_\alpha(0) = 0$, and

$$\tilde{\gamma}_\alpha^\pm = \gamma(\pm\tilde{\omega}_\alpha, \beta_\alpha), \quad (\text{B22})$$

where the dissipator $\mathcal{D}(\hat{O})$ and the dissipation function $\gamma(\omega, \beta)$ are defined in Eqs. (B2) and

(B4). Hence, the global Liouvillian can be expressed as

$$\tilde{\mathcal{L}}_\alpha = \begin{pmatrix} -\tilde{\Gamma}_\alpha^- & 0 & 0 & \tilde{\Gamma}_\alpha^+ \\ 0 & -\frac{1}{2}(\tilde{\Gamma}_\alpha^+ + \tilde{\Gamma}_\alpha^-) + i\tilde{\omega}_\alpha & 0 & 0 \\ 0 & 0 & -\frac{1}{2}(\tilde{\Gamma}_\alpha^+ + \tilde{\Gamma}_\alpha^-) - i\tilde{\omega}_\alpha & 0 \\ \tilde{\Gamma}_\alpha^- & 0 & 0 & -\tilde{\Gamma}_\alpha^+ \end{pmatrix} \quad (\text{B23})$$

with

$$\tilde{\Gamma}_\alpha^\pm = \cos^2(2\theta)\tilde{\gamma}_\alpha^\pm, \quad (\text{B24})$$

the basis is $\left(\tilde{\rho}_{\text{gg}} \quad \tilde{\rho}_{\text{ge}} \quad \tilde{\rho}_{\text{eg}} \quad \tilde{\rho}_{\text{ee}} \right)^T$. For the subsequent analysis, we rewrite the left and right eigenvectors $\langle \tilde{L}_i^\alpha |$ and $| \tilde{R}_i^\alpha \rangle$ of the i th eigenvalue $\tilde{\lambda}_i^\alpha$ as the left and right eigenmatrices

$$\tilde{\sigma}_i^\alpha = \begin{pmatrix} \tilde{\rho}_{\text{gg}} & \tilde{\rho}_{\text{eg}} \\ \tilde{\rho}_{\text{ge}} & \tilde{\rho}_{\text{ee}} \end{pmatrix} \quad (\text{B25})$$

and

$$\tilde{\rho}_i^\alpha = \begin{pmatrix} \tilde{\rho}_{gg} & \tilde{\rho}_{ge} \\ \tilde{\rho}_{eg} & \tilde{\rho}_{ee} \end{pmatrix}, \quad (\text{B26})$$

respectively. The left and right eigenmatrices are bi-orthogonal $\text{Tr}[\tilde{\sigma}_i^\alpha \tilde{\rho}_i^\alpha] = \delta_{i,j}$.

The spectral properties of the global Liouvillian superoperator $\tilde{\mathcal{L}}_\alpha$ can be obtained analytically. The eigenvalues $\tilde{\lambda}_i^\alpha$ are

$$\tilde{\lambda}_0^\alpha = 0, \quad (\text{B27})$$

$$\tilde{\lambda}_1^\alpha = -\frac{1}{2}(\tilde{\Gamma}_\alpha^- + \tilde{\Gamma}_\alpha^+) + i\tilde{\omega}_\alpha, \quad (\text{B28})$$

$$\tilde{\lambda}_2^\alpha = -\frac{1}{2}(\tilde{\Gamma}_\alpha^- - \tilde{\Gamma}_\alpha^+) + i\tilde{\omega}_\alpha, \quad (\text{B29})$$

$$\tilde{\lambda}_3^\alpha = -(\tilde{\Gamma}_\alpha^- + \tilde{\Gamma}_\alpha^+). \quad (\text{B30})$$

In particular, the zero eigenvalue $\tilde{\lambda}_0^\alpha$ corresponds to a stationary state.

Corresponding to the i th eigenvalue $\tilde{\lambda}_i^\alpha$, the left eigenmatrices $\tilde{\sigma}_i^\alpha$ are

$$\tilde{\sigma}_0^\alpha = \begin{pmatrix} 1 & 0 \\ 0 & 1 \end{pmatrix}, \quad (\text{B31})$$

$$\tilde{\sigma}_1^\alpha = \begin{pmatrix} 0 & 0 \\ 1 & 0 \end{pmatrix}, \quad (\text{B32})$$

$$\tilde{\sigma}_2^\alpha = \begin{pmatrix} 0 & 1 \\ 0 & 0 \end{pmatrix}, \quad (\text{B33})$$

$$\tilde{\sigma}_3^\alpha = \begin{pmatrix} \tilde{\Gamma}_\alpha^- & 0 \\ 0 & -\tilde{\Gamma}_\alpha^+ \end{pmatrix}. \quad (\text{B34})$$

The right eigenmatrices $\tilde{\sigma}_i^\alpha$ are

$$\tilde{\rho}_0^\alpha = \frac{1}{\tilde{\Gamma}_\alpha^- + \tilde{\Gamma}_\alpha^+} \begin{pmatrix} \tilde{\Gamma}_\alpha^+ & 0 \\ 0 & \tilde{\Gamma}_\alpha^- \end{pmatrix}, \quad (\text{B35})$$

$$\tilde{\rho}_1^\alpha = \begin{pmatrix} 0 & 1 \\ 0 & 0 \end{pmatrix}, \quad (\text{B36})$$

$$\tilde{\rho}_2^\alpha = \begin{pmatrix} 0 & 0 \\ 1 & 0 \end{pmatrix}, \quad (\text{B37})$$

$$\tilde{\rho}_3^\alpha = \frac{1}{\tilde{\Gamma}_\alpha^- + \tilde{\Gamma}_\alpha^+} \begin{pmatrix} 1 & 0 \\ 0 & -1 \end{pmatrix}. \quad (\text{B38})$$

The right eigenmatrix $\tilde{\sigma}_0^\alpha$ is the equilibrium steady state in each isochoric process α ($\alpha = \text{h, c}$), corresponding to the zero eigenvalue $\tilde{\lambda}_0^\alpha$ of the global Liouvillian superoperator $\tilde{\mathcal{L}}$. Obviously, it is a thermalized equilibrium state and exhibits properties similar to those of the Gibbs state. Hence, in the main text, we focus on the global master equation, which properly incorporates the system eigenstructure and yields physically consistent steady-cycle behavior.

-
- [1] S. Bhattacharjee and A. Dutta, Quantum thermal machines and batteries, *The European Physical Journal B* **94**, 239 (2021).
- [2] V. Mukherjee and U. Divakaran, Many-body quantum thermal machines, *Journal of Physics: Condensed Matter* **33**, 454001 (2021).
- [3] P. P. Hofer, J. B. Brask, M. Perarnau-Llobet, and N. Brunner, Quantum Thermal Machine as a Thermometer, *Phys. Rev. Lett.* **119**, 090603 (2017).

- [4] D. Newman, F. Mintert, and A. Nazir, Quantum limit to nonequilibrium heat-engine performance imposed by strong system-reservoir coupling, *Phys. Rev. E* **101**, 052129 (2020).
- [5] R. Uzdin, A. Levy, and R. Kosloff, Equivalence of Quantum Heat Machines, and Quantum-Thermodynamic Signatures, *Phys. Rev. X* **5**, 031044 (2015).
- [6] Y. Xiao, D. Liu, J. He, Y. Ma, Z. Wu, and J. Wang, Quantum Otto engine with quantum correlations, *Phys. Rev. A* **108**, 042614 (2023).
- [7] M. Kaneyasu and Y. Hasegawa, Quantum Otto cycle under strong coupling, *Phys. Rev. E* **107**, 044127 (2023).
- [8] M. Herrera, J. H. Reina, I. D'Amico, and R. M. Serra, Correlation-boosted quantum engine: A proof-of-principle demonstration, *Phys. Rev. Res.* **5**, 043104 (2023).
- [9] G. Piccitto, M. Campisi, and D. Rossini, The Ising critical quantum Otto engine, *New Journal of Physics* **24**, 103023 (2022).
- [10] H.-G. Xu, J. Jin, G. D. M. Neto, and N. G. de Almeida, Universal quantum Otto heat machine based on the Dicke model, *Phys. Rev. E* **109**, 014122 (2024).
- [11] R. Kosloff and Y. Rezek, The Quantum Harmonic Otto Cycle, *Entropy* **19**, 10.3390/e19040136 (2017).
- [12] R. Kosloff and A. Levy, Quantum Heat Engines and Refrigerators: Continuous Devices, *Annual Review of Physical Chemistry* **65**, 365 (2014).
- [13] J. Roßnagel, O. Abah, F. Schmidt-Kaler, K. Singer, and E. Lutz, Nanoscale Heat Engine Beyond the Carnot Limit, *Phys. Rev. Lett.* **112**, 030602 (2014).
- [14] T. Feldmann and R. Kosloff, Quantum four-stroke heat engine: Thermodynamic observables in a model with intrinsic friction, *Phys. Rev. E* **68**, 016101 (2003).
- [15] G. P. Beretta, Quantum thermodynamic Carnot and Otto-like cycles for a two-level system,

- Europhysics Letters **99**, 20005 (2012).
- [16] O. Abah and E. Lutz, Optimal performance of a quantum Otto refrigerator, Europhysics Letters **113**, 60002 (2016).
- [17] A. Solfanelli, M. Falsetti, and M. Campisi, Nonadiabatic single-qubit quantum Otto engine, Phys. Rev. B **101**, 054513 (2020).
- [18] M. Ishizaki, N. Hatano, and H. Tajima, Switching the function of the quantum Otto cycle in non-Markovian dynamics: Heat engine, heater, and heat pump, Phys. Rev. Res. **5**, 023066 (2023).
- [19] V. Mehta and R. S. Johal, Quantum Otto engine with exchange coupling in the presence of level degeneracy, Phys. Rev. E **96**, 032110 (2017).
- [20] S. Chakraborty, A. Das, and D. Chruściński, Strongly coupled quantum Otto cycle with single qubit bath, Phys. Rev. E **106**, 064133 (2022).
- [21] A. Hewgill, A. Ferraro, and G. De Chiara, Quantum correlations and thermodynamic performances of two-qubit engines with local and common baths, Phys. Rev. A **98**, 042102 (2018).
- [22] G. Thomas and R. S. Johal, Coupled quantum Otto cycle, Phys. Rev. E **83**, 031135 (2011).
- [23] M. F. Anka, T. R. de Oliveira, and D. Jonathan, Work and efficiency fluctuations in a quantum Otto cycle with idle levels, Phys. Rev. E **109**, 064129 (2024).
- [24] J. Gao and N. Hatano, Maximum power of coupled-qubit Otto engines, Phys. Rev. Res. **6**, 023172 (2024).
- [25] E. A. Ivanchenko, Quantum Otto cycle efficiency on coupled qudits, Phys. Rev. E **92**, 032124 (2015).
- [26] O. Raz, Y. Subaşı, and C. Jarzynski, Mimicking Nonequilibrium Steady States with Time-Periodic Driving, Phys. Rev. X **6**, 021022 (2016).

- [27] J. Freitas and M. Esposito, Emergent second law for non-equilibrium steady states, *Nature Communications* **13**, 5084 (2022).
- [28] G. Guarnieri, G. T. Landi, S. R. Clark, and J. Goold, Thermodynamics of precision in quantum nonequilibrium steady states, *Phys. Rev. Res.* **1**, 033021 (2019).
- [29] P. P. Hofer, M. Perarnau-Llobet, L. D. M. Miranda, G. Haack, R. Silva, J. B. Brask, and N. Brunner, Markovian master equations for quantum thermal machines: local versus global approach, *New Journal of Physics* **19**, 123037 (2017).
- [30] S. Scali, J. Anders, and L. A. Correa, Local master equations bypass the secular approximation, *Quantum* **5**, 451 (2021).
- [31] M. Cattaneo, G. L. Giorgi, S. Maniscalco, and R. Zambrini, Local versus global master equation with common and separate baths: superiority of the global approach in partial secular approximation, *New Journal of Physics* **21**, 113045 (2019).
- [32] N. Shiraishi, K. Saito, and H. Tasaki, Universal Trade-Off Relation between Power and Efficiency for Heat Engines, *Phys. Rev. Lett.* **117**, 190601 (2016).
- [33] P. Pietzonka and U. Seifert, Universal Trade-Off between Power, Efficiency, and Constancy in Steady-State Heat Engines, *Phys. Rev. Lett.* **120**, 190602 (2018).
- [34] H. Breuer and F. Petruccione, *The Theory of Open Quantum Systems* (Oxford University Press, 2002).